

N84-34392

SPACE RADIATION LABORATORY  
CALIFORNIA INSTITUTE OF TECHNOLOGY  
Pasadena, California 91125

SEMI-ANNUAL STATUS REPORT

for

NATIONAL AERONAUTICS AND SPACE ADMINISTRATION  
Grant NGR 05-002-160\*  
"RESEARCH IN PARTICLES AND FIELDS"

for

1 April 1983 - 31 March 1984

E. C. Stone, Principal Investigator  
A. Buffington, Coinvestigator  
L. Davis, Jr., Coinvestigator  
T. A. Prince, Coinvestigator  
R. E. Vogt, Coinvestigator

\*NASA Technical Officer: Dr. J. F. Ormes, High Energy Astrophysics

Table of Contents

1. Cosmic Rays and Astrophysical Plasmas .....	3
1.1. Activities in Support of or in Preparation for Spacecraft Experiments ....	3
1.1.1. The High Energy Isotope Spectrometer Telescope (HEIST) .....	3
1.2. Experiments on NASA Spacecraft .....	11
1.2.1. An Electron/Isotope Spectrometer (EIS) Launched on IMP-7 on 22 September 1972 and on IMP-8 on 26 October 1973 .....	11
A Search for $^2\text{H}$ , $^3\text{H}$ , and $^3\text{He}$ in Large Solar Flares .....	12
1.2.2. An Interstellar Cosmic Ray and Planetary Magnetospheres Experiment for the Voyager Missions Launched in 1977 .....	15
Studies of Low Energy Cosmic Rays - The Anomalous Component .....	16
1.2.3. A Heavy Isotope Spectrometer Telescope (HIST) Launched on ISEE-3 in August 1978 .....	20
The Isotopic Composition of the Anomalous Low-Energy Cosmic Rays .....	21
1.2.4. A Heavy Nuclei Experiment (HNE) Launched on HEAO-C in September 1979 .....	26
Cosmic Ray Abundances of the Platinum-Lead Elements .....	27
1.2.5. A Magnetometer Experiment on Pioneer 11 .....	29
1.2.6. Proposal for an Advanced Composition Explorer (ACE) .....	29
2. Gamma Rays .....	31
2.1. Activities in Support of or in Preparation for Spacecraft Experiments ....	31
2.1.1. A Balloon-Borne Gamma Ray Imaging Payload (GRIP) .....	31
2.1.2. Development of Large Anger Camera Detectors for $\gamma$ -ray Astronomy .	33
2.1.3. Technology Development .....	36
2.2. Experiments on NASA Spacecraft .....	37
2.2.1. The Gamma Ray Spectrometer Experiment on the Solar Maximum Mission .....	37
3. Other Activities .....	39
4. Bibliography .....	40

## SEMI-ANNUAL STATUS REPORT

NASA Grant NGR 05-002-160

Space Radiation Laboratory (SRL)  
California Institute of Technology

1 April 1983 - 31 March 1984

This report covers the research activities in Cosmic Rays, Gamma Rays, and Astrophysical Plasmas supported under NASA Grant NGR 05-002-160. The report is divided into sections which describe the activities, followed by a bibliography.

This group's research program is directed toward the investigation of the astrophysical aspects of cosmic rays and gamma rays and of the radiation and electromagnetic field environment of the Earth and other planets. We carry out these investigations by means of energetic particle and photon detector systems flown on spacecraft and balloons.

### 1. Cosmic Rays and Astrophysical Plasmas

This research program is directed toward the investigation of galactic, solar, interplanetary, and planetary energetic particles and plasmas. The emphasis is on precision measurements with high resolution in charge, mass, and energy. The main efforts of this group, which are supported partially or fully by this grant, have been directed toward the following two categories of experiments.

#### 1.1. Activities in Support of or in Preparation for Spacecraft Experiments

These activities generally embrace prototypes of experiments on existing or future NASA spacecraft or they complement and/or support such observations.

##### 1.1.1. The High Energy Isotope Spectrometer Telescope (HEIST)

HEIST is a large area ( $0.25 \text{ m}^2\text{sr}$ ) balloon-borne isotope spectrometer designed to make high-resolution measurements of isotopes in the element range from neon to nickel ( $10 \leq Z \leq 28$ ) at energies of about 2 GeV/nucleon. The instrument consists of a stack of 12 NaI(Tl) scintillators, two Cerenkov counters (C1 and C2), and two plastic scintillators (S1 and S2) as illustrated in Figure 1. Each of the 2-cm thick NaI disks is viewed by six 1.5-inch photomultipliers whose combined outputs measure the energy deposition in that layer. In addition, the six outputs from each disk are compared to determine the position at which incident nuclei traverse each layer to an accuracy of  $\sim 2 \text{ mm}$ . The Cerenkov counters, which measure particle velocity, are each viewed by twelve 5-inch photomultipliers using light integration boxes. This is a collaborative effort with the Danish Space Research Institute.

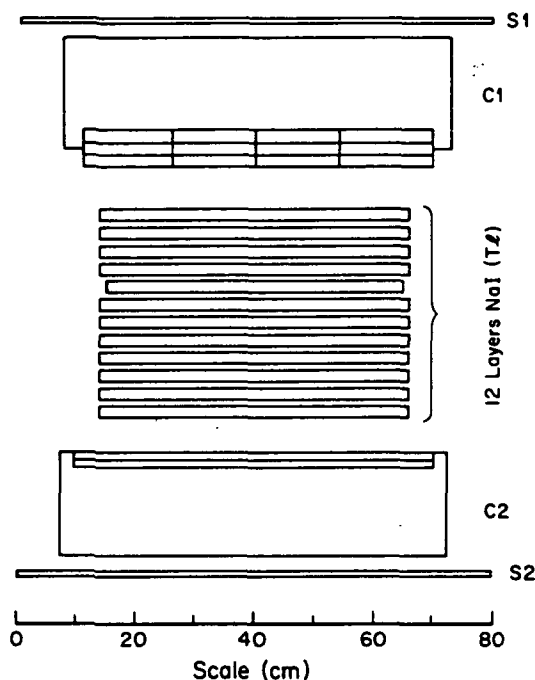


Figure 1

HEIST determines the mass of individual nuclei by measuring both the change in the Lorentz factor ( $\Delta\gamma$ ) that results from traversing the NaI stack, and the energy loss ( $\Delta E$ ) in the stack. Since the total energy of an isotope is given by  $E = \gamma M$ , the mass  $M$  can be determined by  $M = \Delta E / \Delta\gamma$ . The instrument is designed to achieve a typical mass resolution of 0.2 amu.

In November of 1982 the flight sensor system was calibrated during a limited exposure to a  $^{55}\text{Mn}$  beam. This calibration provided data for mapping of the NaI scintillators and the aerogel counter. Figure 2 shows a color example of the response from one of the six tubes from a single layer. Clearly visible is the gradual gradient in light collection as a function of distance from the tube. Also visible at the sides are "blind" regions from which only scattered or reflected light can reach the tube. This response has been modeled using the optical properties of the materials. The ratio of the response of two opposite tubes provides accurate position information, as shown in Figure 3. Although the Mn point deviates from the performance expected from photoelectron statistics alone, the achieved value of 1.3 mm rms is better than required.

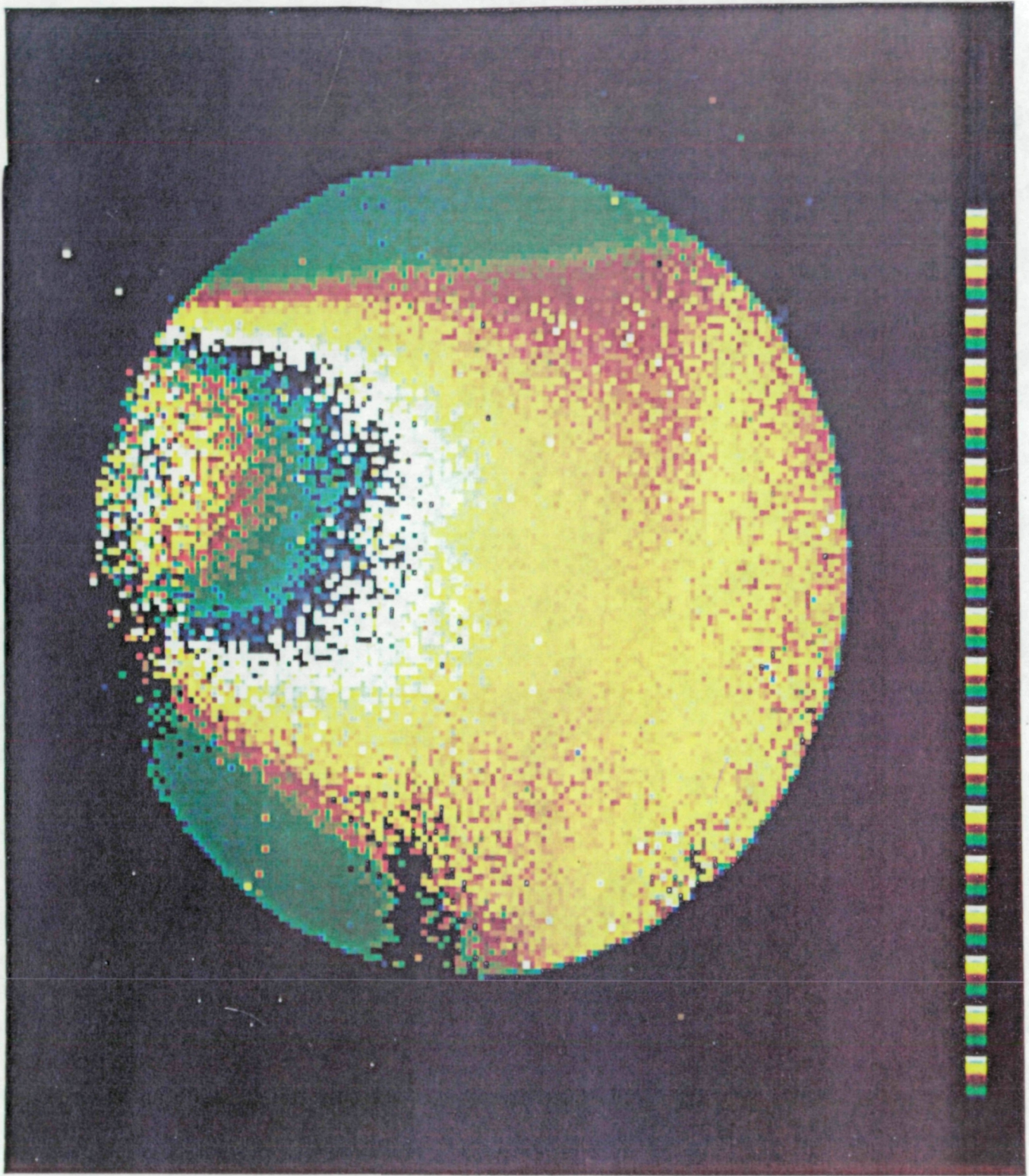


Figure 2 Color-coded map of the light intensity measured by a single photomultiplier viewing a NaI disk, as measured with  $^{55}\text{Mn}$  ions. The light intensity varies by a factor of  $\sim 10$  from just in front to directly opposite the tube. Note the sharp boundaries outside of which only reflected or scattered light can reach the tube.

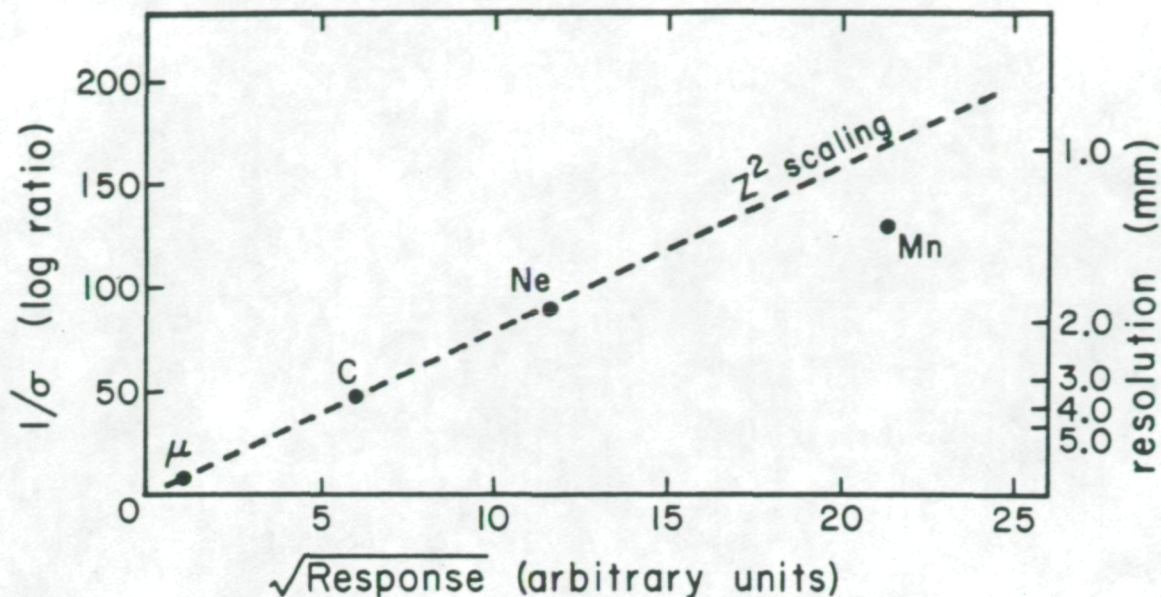


Figure 3

In Figure 4 we show a color-map of the combined response of six tubes from a layer. While there are gradients in response near the counter edges, they can be removed by mapping, using the ratios of the outputs of the phototubes as coordinates. Although the mapping of the NaI stack is not complete, Figure 5 shows a histogram of the relative response to  $^{55}\text{Mn}$ , with  $\gamma \approx 2.7$  in one layer, including preliminary mapping corrections. The width of the distribution is 1.0% rms compared to an expected width due to Landau fluctuations of 0.7% rms. This indicates a residual 0.7% uncertainty due to mapping inaccuracies and photoelectron statistics. Assuming a comparable uncertainty in each of the subsequent layers, we would expect a resulting uncertainty of  $\sim 0.2\%$  in the total energy of a typical particle stopping in layer 10. This would contribute  $\sim 0.1$  amu to a measurement of the mass of  $^{55}\text{Mn}$ , and a correspondingly smaller amount to lighter nuclei.

The  $^{55}\text{Mn}$  Bevalac run also provided data for mapping of the aerogel Cerenkov counter (C1), as can be seen in Figure 6, which shows the summed response of all twelve tubes to  $^{55}\text{Mn}$ . The boundaries of the 14 cm x 14 cm aerogel blocks are clearly visible. A preliminary analysis indicates that the response variations over  $>75\%$  of the area are below the design goal of 2%/cm (the color scale corresponds to 1% per color level). For example, a trajectory accuracy of 2 mm, combined with a 2%/cm gradient gives a mass uncertainty of  $\sim 0.05$  amu for  $^{55}\text{Mn}$  with  $\gamma=2.75$ . Figure 7 shows the response to  $^{55}\text{Mn}$  after mapping corrections have been applied. Note that there are small regions near the counter edge for which no mapping data was obtained; these will be mapped using relativistic C and O nuclei obtained in-flight.

Figure 8 shows the relative response of Cerenkov counters C1 (curve a) and C2 (curve b) as a function of  $\gamma$ . By fitting the Cerenkov response measured in C1 during runs with different energy  $^{55}\text{Mn}$  beams, it was determined that the aerogel counters produce an average of  $23 \pm 4$  photoelectrons for a relativistic  $Z=1$  particle at normal incidence. The amount of light produced at energies below threshold ( $\gamma \approx 2.3$ ) was found to be 3.6% of the  $\beta=1$  light yield. Of this, we expect 2.8% to be due to delta rays and to Cerenkov light from the  $\text{BaSO}_4$  paint grains, giving an upper limit of 1% for the

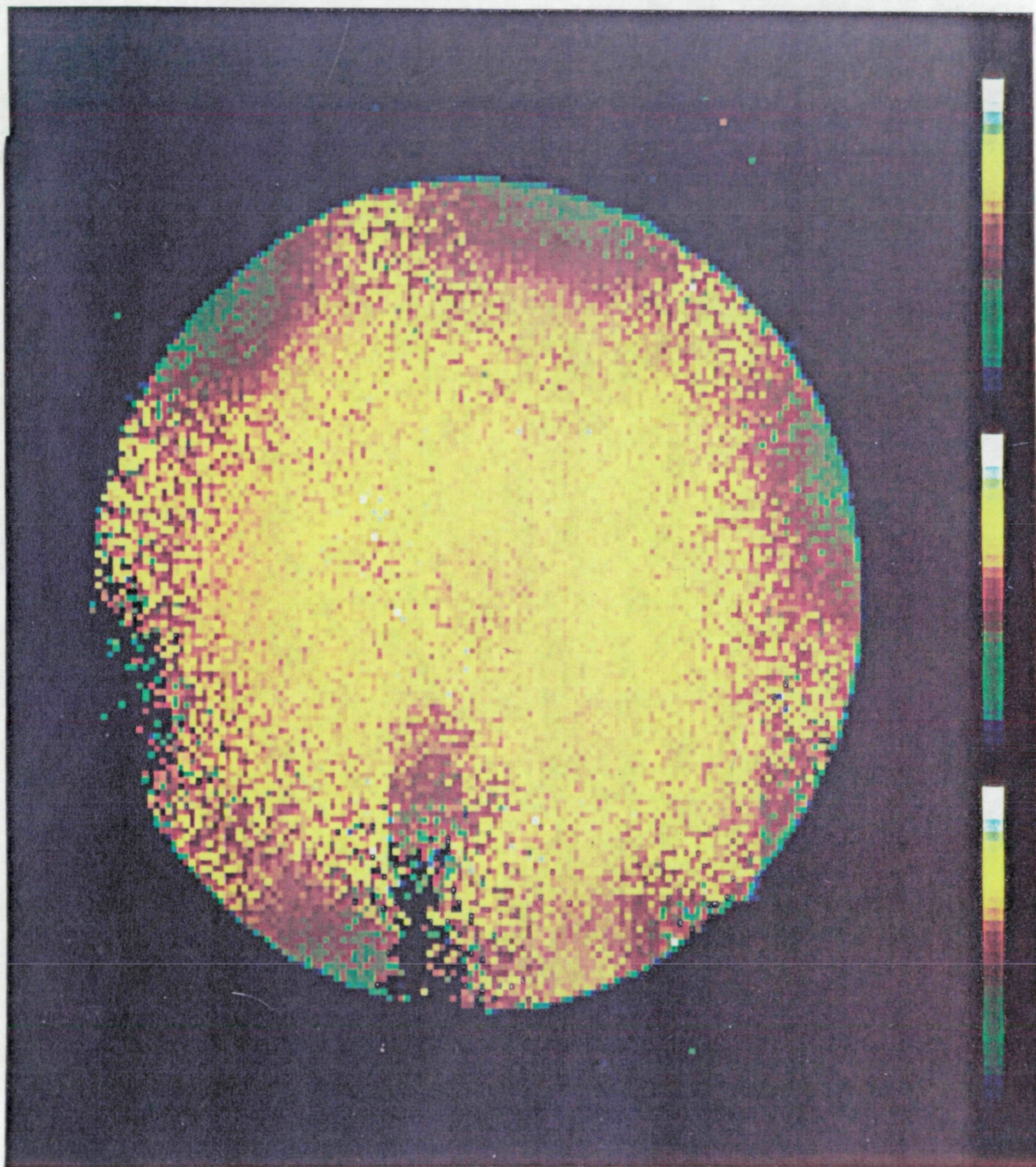


Figure 4 Color-coded map of the light intensity obtained from the sum of 6 phototubes viewing a single NaI layer, as measured with  $^{56}\text{Mn}$  ions.

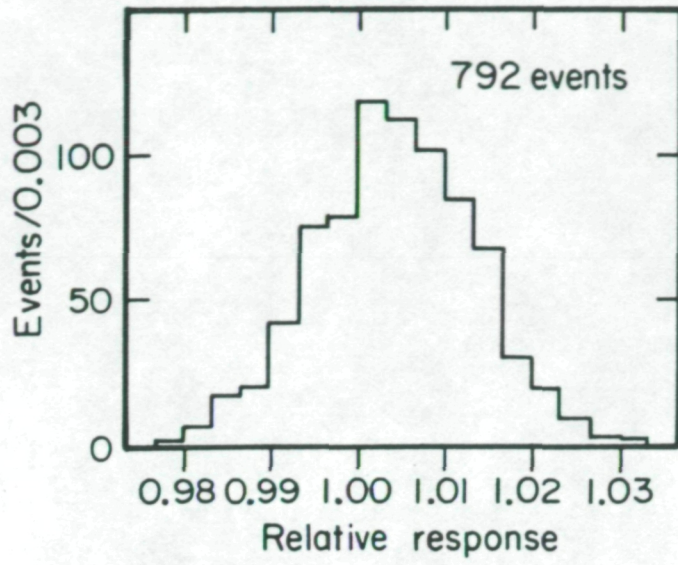


Figure 5

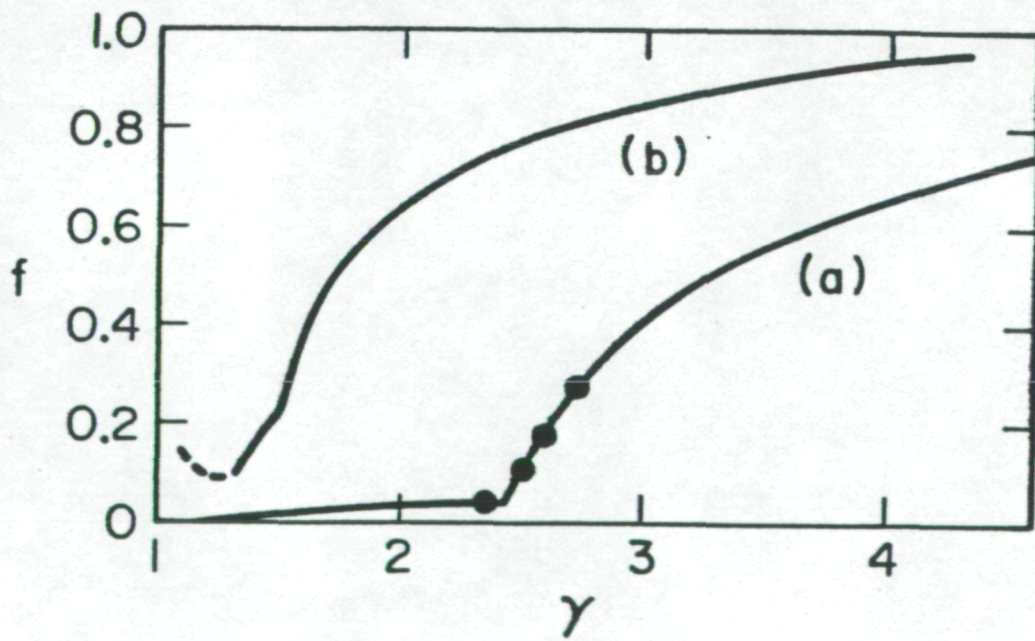


Figure 8

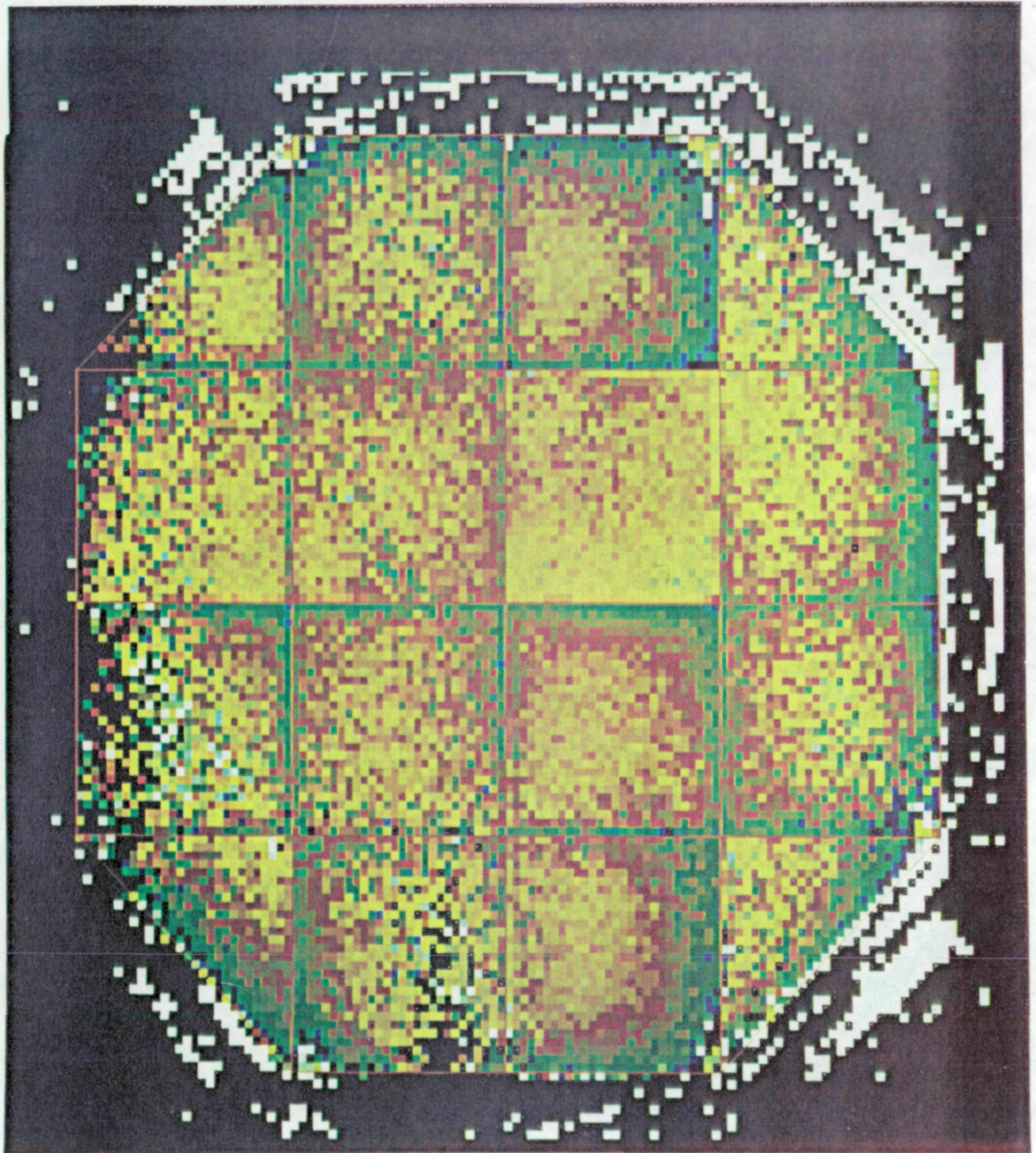


Figure 6 Color map of the uncorrected response of the top Cerenkov counter to  $^{65}\text{Mn}$  ions with  $\gamma \approx 2.75$ . Note the boundaries of the aerogel blocks.

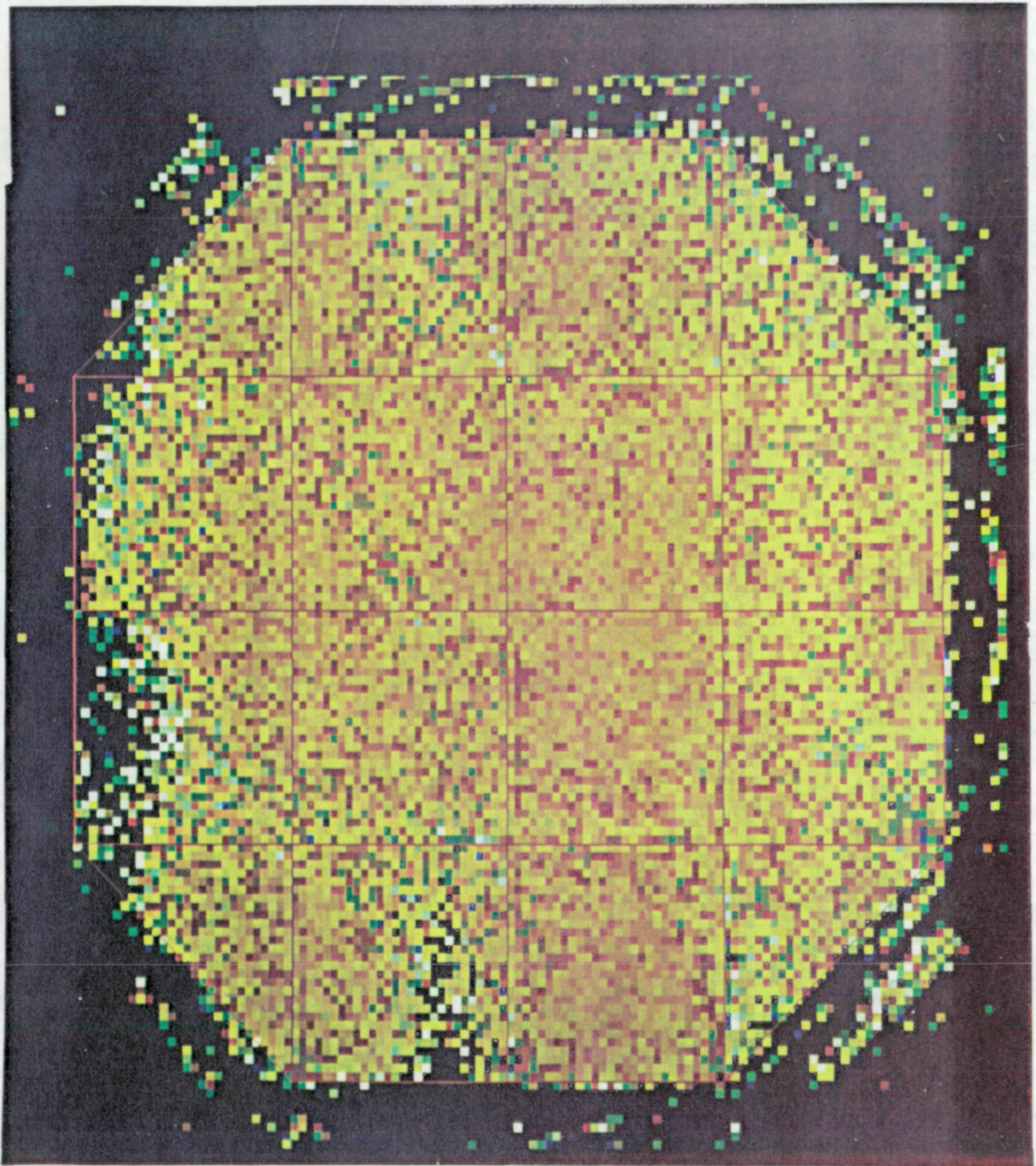


Figure 7 Color map of the corrected response of the top Cerenkov counter. The corrections were determined from fits to the response in Figure 6.

amount of scintillation light produced in the aerogels. An upper limit to small-scale variations in the index of refraction of the aerogels was found to be  $\Delta n < 0.0003$ , which would result in a maximum error of  $\delta M \approx 0.08$  amu for  $^{55}\text{Mn}$ , and less for lighter nuclei.

The entire balloon flight system is now fully integrated and undergoing pre-flight checks in Palestine, Texas in preparation for a flight of 40 hours or more during the Spring 1984 high-altitude wind turn-around. This flight will provide a proof of this approach for high-energy cosmic-ray isotope spectroscopy, and it should provide the first direct measurements of some of the abundant isotopes at energies of  $\sim 2$  GeV/nucleon.

The following talks and papers have been presented lately:

- "A Cerenkov -  $dE/dX$  Experiment for Measuring Cosmic-Ray Isotopes from Neon Through Iron," A. Buffington et al., *Proceedings of 18th International Cosmic Ray Conference, Bangalore, India 2*, 49-52 (1983).
- "Further Analysis of a Recent Cosmic-Ray Antiproton Experiment," A. Buffington and S. M. Schindler, *Proceedings of 18th International Cosmic Ray Conference, Bangalore, India 2*, 71-74 (1983).
- "Calibration of An Aerogel Counter of Index 1.1 at the Bevalac," I. L. Rasmussen et al., *Proceedings of 18th International Cosmic Ray Conference, Bangalore, India 8*, 77-80 (1983).
- "Calibration of a Stack of NaI Scintillators at the Berkeley Bevalac," S. M. Schindler et al., *Proceedings of 18th International Cosmic Ray Conference, Bangalore, India 8*, 73-76 (1983).

## 1.2. Experiments on NASA Spacecraft

The SR&T grant program of the Space Radiation Laboratory is strengthened by and contributes to the other programs described here. Activities related to these programs are primarily funded by mission-related contracts but grant funds are used to provide a general support base and the facilities which make these programs possible.

### 1.2.1. An Electron/Isotope Spectrometer (EIS) Launched on IMP-7 on 22 September 1972 and on IMP-8 on 26 October 1973

This experiment is designed to measure the energy spectra of electrons and positrons (0.16 to  $\sim 6$  MeV), and the differential energy spectra of the nuclear isotopes of hydrogen, helium, lithium, and beryllium ( $\sim 2$  to 50 MeV/nucleon). In addition, it provides measurements of the fluxes of the isotopes of carbon, nitrogen, and oxygen from  $\sim 5$  to  $\sim 15$  MeV/nucleon. The measurements from this experiment support studies of the origin, propagation, and solar modulation of galactic cosmic rays; the acceleration and propagation of solar flare and interplanetary particles; and the origin and transport of energetic magnetospheric particles observed in the plasma sheet, adjacent to the magnetopause, and upstream of the bow shock.

The extensive EIS data set has been utilized in comprehensive studies of solar, interplanetary, and magnetospheric processes. Correlative studies have involved data from other IMP investigations and from other spacecraft, as well as direct comparisons of EIS data from IMP-7 and IMP-8. In particular, we are currently using IMP data to support a multidisciplinary workshop that is studying cosmic ray modulation and the large scale structure of the heliosphere.

The following recent talks and papers have been presented.

- "Microstructure of Magnetic Reconnection in Earth's Magnetotail," J. W. Bieber et al., *J. Geophys. Res.* (submitted for 1984).
- "A Search for Deuterium, Tritium and  $^3\text{He}$  in Large Solar Flares," R.A. Mewaldt and E.C. Stone, *Bull. Am. Phys. Soc.* **28**, 742 (1983).
- "Cosmic Ray  $^2\text{H}$ ,  $^3\text{H}$ , and Anomalous H and He Nuclei," E.C. Stone and R.A. Mewaldt, *Bull. Am. Phys. Soc.* **28**, 742 (1983).
- "A Search for  $^2\text{H}$ ,  $^3\text{H}$ , and  $^3\text{He}$  in Large Solar Flares," R. A. Mewaldt and E. C. Stone, *Proceedings of 18th International Cosmic Ray Conference, Bangalore, India* **4**, 52-55 (1983).
- "Deuterium,  $^3\text{He}$ , and Anomalous H and He Nuclei," R.A. Mewaldt and E.C. Stone, *Proceedings of 18th International Cosmic Ray Conference, Bangalore, India* **2**, 42 (1983).
- "The Isotopic Composition of the Anomalous Low-Energy Cosmic Rays," R.A. Mewaldt et al., *Ap. J.* (1983 Submitted).
- "A Search for  $^2\text{H}$ ,  $^3\text{H}$ , and  $^3\text{He}$  in Large Solar Flares," R.A. Mewaldt and E.C. Stone, *EOS Tran. AGU Nov.* **64**, 791 (1983).

A summary of one of these studies is given below. A second study based on both IMP and ISEE-3 data is summarized in section 1.2.3.

### A Search for $^2\text{H}$ , $^3\text{H}$ , and $^3\text{He}$ in Large Solar Flares

The rare isotopes  $^2\text{H}$ ,  $^3\text{H}$ , and  $^3\text{He}$  are produced by nuclear interactions of accelerated  $^1\text{H}$  and  $^4\text{He}$  nuclei as they pass through the solar atmosphere. Earlier studies of solar energetic particles (SEPs) have reported finite abundances of each these isotopes in data summed over many large flares, as well as enhanced abundances of  $^3\text{He}$  in so-called " $^3\text{He}$ -rich" events. Although the finite  $^2\text{H}$  and  $^3\text{H}$  observations require that SEPs have traversed  $\sim 0.1$  to  $\sim 1$  g/cm<sup>2</sup>, at least one theoretical model requires that SEPs traverse  $\leq 1\%$  of this amount during acceleration. Motivated by this apparent discrepancy, we have re-examined the evidence for nuclear reaction products in SEPs in a new study that includes essentially all large solar particle events observed at 1 AU from 1974 to 1979. The results of this study imply that earlier observations have significantly overestimated the abundance of  $^2\text{H}$ ,  $^3\text{H}$ , and  $^3\text{He}$  in large solar flares. We find no evidence that solar flare nuclei have suffered any significant amount of fragmentation before escaping from the Sun.

The observations were made with the Caltech Electron/Isotope Spectrometers on IMP-7 and IMP-8 and include IMP-8 data from 1/74 to 12/79 and IMP-7 data from

1/74 to 6/78. Fig. 9 shows the H-isotope data from IMP-8. The  $^1\text{H}$  mass resolution of 0.048 amu agrees with that expected and is the best ever achieved to our knowledge. Note that within the limits in which 95% of all real  $^2\text{H}$  and  $^3\text{H}$  would fall there are only 2 (for  $^2\text{H}$ ) and 3 (for  $^3\text{H}$ ) events, and considering the relatively smooth background level, no evidence for a finite flux of either  $^2\text{H}$  or  $^3\text{H}$ . In the IMP-7 data there is only 1 event with mass  $> 1.5$  amu. Summing the IMP-7 and IMP-8 data, and taking into account the observed background distribution and the GCR  $^2\text{H}$  flux, we find the 95% confidence upper limits summarized in Table 1.

In Fig. 10 we show the He mass distribution from both instruments, where two  $^3\text{He}$ -rich flares previously identified by other groups are shown separately. In the bottom two panels there is no convincing evidence for  $^3\text{He}$  ( $\sim 2$  GCR  $^3\text{He}$  are expected). Table 1 includes the resulting  $^3\text{He}/^4\text{He}$  upper limit from IMP-7 and IMP-8 combined, and a finite ratio for the total data sample (including the 2  $^3\text{He}$ -rich flares).

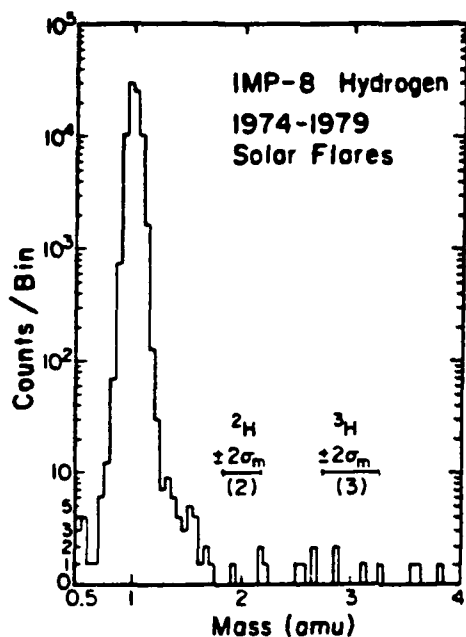


Figure 9

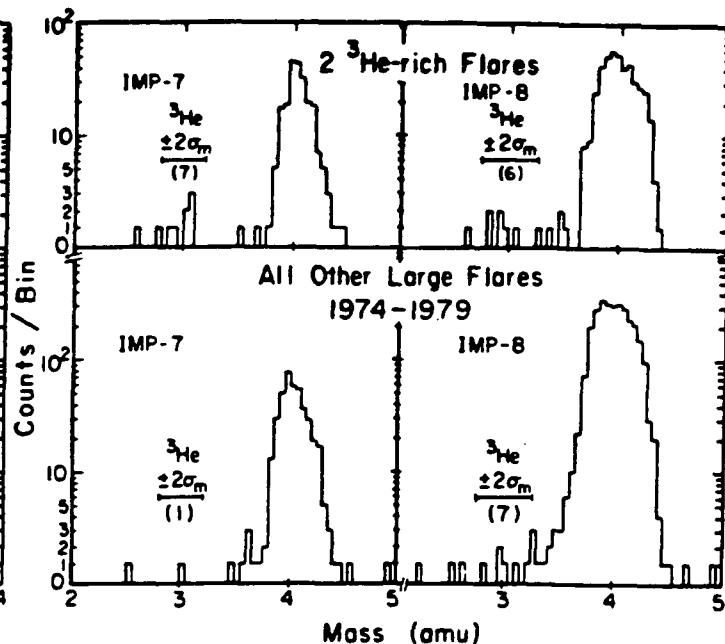


Figure 10

In Figs. 11, 12, and 13 we compare our results with earlier measurements. Note that our upper limits for both  $^2\text{H}/^1\text{H}$  and  $^3\text{H}/^1\text{H}$  are significantly lower than the IMP-5 and IMP-6 finite measurements at essentially the same energy/nuc. There also appear to be significant experimental differences for  $^3\text{He}/^4\text{He}$ .

For  $^3\text{He}/^4\text{He}$ , which is known to vary by orders of magnitude from flare to flare, we cannot exclude the possibility that sampling effects might explain the large differences evident in Fig. 11, if e.g., the earlier studies happened to include more  $^3\text{He}$ -rich flares (such  $^3\text{He}$  enhancements are no longer attributed to nuclear interactions). However, our new measurements, those from Pioneer-10, and our ISEE-3 data lead us to conclude that typical large solar events have a  $^3\text{He}/^4\text{He}$  ratio at  $\sim 20$  MeV/nuc which is considerably lower than indicated by earlier studies.

In the case of  $^2\text{H}$  and  $^3\text{H}$ , it does not appear possible that flare-sampling differences could explain the discrepancies evident at  $\sim 10$  MeV/nuc, since there was no evidence for flare-to-flare variations in the IMP-5  $^2\text{H}/^1\text{H}$  and  $^3\text{H}/^1\text{H}$  ratios, and since the IMP-6 data typically included  $\sim 20$   $^2\text{H} + ^3\text{H}$  events from each flare studied, so that flare-to-flare variations of the required magnitude (factor of  $> 10$ ) would have been easily detectable. Another possibility is that the IMP-5 and IMP-6 results include substantial  $^2\text{H}$  and  $^3\text{H}$  produced by nuclear interactions within the instruments.

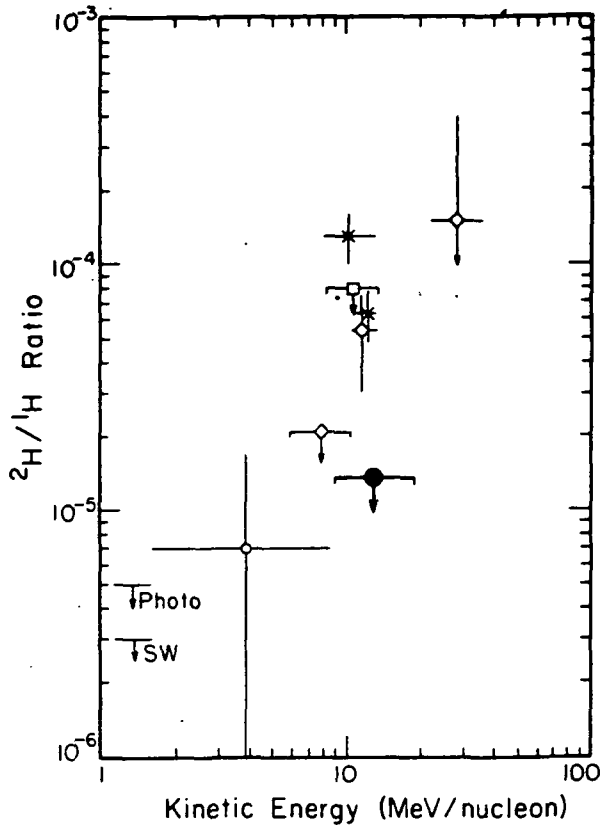


Figure 11

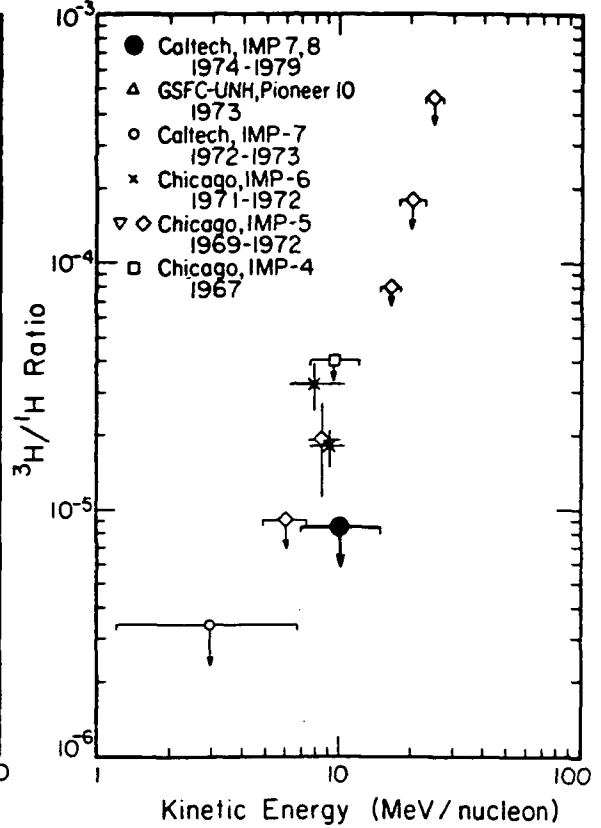
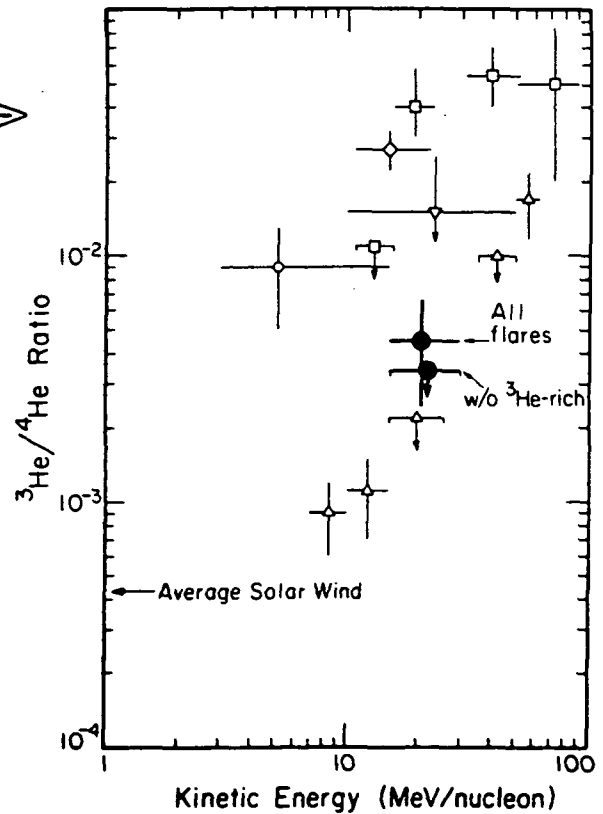


Figure 12

Figure 13 →

Table 1 - Solar Flare Isotope Ratios

Isotope Abundance Ratio	Energy Interval (MeV/nuc)	86% Confidence Interval or 95% Confidence Upper Limit
$^2\text{H}/^1\text{H}$	9-19	$< 1.4 \times 10^{-5}$
$^2\text{H}/^4\text{He}$	9-19	$< 9 \times 10^{-4}$
$^3\text{H}/^1\text{H}$	7-15	$< 9 \times 10^{-6}$
$^3\text{H}/^4\text{He}$	7-15	$< 6 \times 10^{-4}$
$^3\text{He}/^1\text{H}$ (w/o $^3\text{He}$ -rich)	15-30	$< 4 \times 10^{-5}$
$^3\text{He}/^4\text{He}$ (w/o $^3\text{He}$ -rich)	15-30	$< 3.4 \times 10^{-3}$
$^3\text{He}/^4\text{He}$ (all flares)	15-30	$4.5^{+2.3}_{-2.1} \times 10^{-3}$
$^4\text{He}/^1\text{H}$	13-24	$1.3 \times 10^{-2}$



The results reported here indicate that the typical particle escaping from the Sun has not traversed any substantial amount of material, thus removing this constraint from solar flare acceleration models. From the "thin-target" model of Ramaty and Kozlovsky (which neglects  $dE/dx$  losses), and our  ${}^2\text{H}/{}^1\text{H}$  upper limit, we estimate an upper limit to the average pathlength ( $x$ ) of  $x < 50 \text{ mg/cm}^2$  at 50 MeV, the typical energy for producing  ${}^2\text{H}$  and  ${}^3\text{H}$  in our energy interval. An even smaller limit ( $x < 30 \text{ mg/cm}^2$ ) results from a more realistic model by Anglin that includes  $dE/dx$  losses.

Although recent solar flare  $\gamma$ -ray observations provide conclusive evidence that nuclear reactions occur during solar flares, such  $\gamma$ -rays are believed to result mainly from nuclei that slow down and stop in the solar atmosphere, rather than from nuclei that escape the Sun. Thus from the work of Ramaty it can be estimated that for  $x = 30 \text{ mg/cm}^2$ , interactions involving particles that escape into interplanetary space would account for  $< 1\%$  of the  $\gamma$ -rays produced in the June 7, 1980 event. It is likely that the actual pathlength is much less, in which case much larger data samples will be required to detect directly high-energy nuclear-interaction products such as  ${}^2\text{H}$  and  ${}^3\text{H}$ .

### 1.2.2. An Interstellar Cosmic Ray and Planetary Magnetospheres Experiment for the Voyager Missions Launched in 1977.

This experiment is conducted by this group in collaboration with F. B. McDonald, J. H. Trainor, and A. W. Schardt (Goddard Space Flight Center), W. R. Webber (University of New Hampshire), and J. R. Jokipii (University of Arizona), and has been designated the Cosmic Ray Subsystem (CRS) for the Voyager Missions. The experiment is designed to measure the energy spectra, elemental and (for lighter elements) isotopic composition, and streaming patterns of cosmic-ray nuclei from H to Fe over an energy range of 0.5 to 500 MeV/nucleon and the energy spectra of electrons with 3 - 100 MeV. These measurements will be of particular importance to studies of stellar nucleosynthesis, and of the origin, acceleration, and interstellar propagation of cosmic rays. Measurements of the energy spectra and composition of energetic particles trapped in the magnetospheres of the outer planets are used to study their origin and relationship to other physical phenomena and parameters of those planets. Measurements of the intensity and directional characteristics of solar and galactic energetic particles as a function of the heliocentric distance will be used for *in situ* studies of the interplanetary medium and its boundary with the interstellar medium. Measurements of solar energetic particles are crucial to understanding solar composition and solar acceleration processes.

The CRS flight units on both Voyager spacecraft have been operating successfully since the launches on August 20, 1977 and September 5, 1977. The CRS team participated in the Voyager 1 and 2 Jupiter encounter operations in March and July 1979, and in the Voyager 1 and 2 Saturn encounters in November 1980 and August 1981. The Voyager data represent an immense and diverse data base, and a number of scientific problems are under analysis. These investigation topics range from the study of galactic particles to particle acceleration phenomena in the interplanetary medium, to plasma/field energetic particle interactions, to acceleration processes on the sun, to studies of elemental abundances of solar, planetary, interplanetary, and galactic energetic particles, and to studies of particle/field/satellite interactions in the magnetospheres of Jupiter and Saturn.

The following publications and papers for scientific meetings, based on Voyager data, were generated:

- "Short and Long Term Variations of the Anomalous Component," A.C. Cum-

mings et al., *Proceedings of 18th International Cosmic Ray Conference, Bangalore, India* (1983 in press).

- "Studies of Low Energy Cosmic Rays - The Anomalous Component," W.R. Webber et al., *Proceedings of 18th International Cosmic Ray Conference, Bangalore, India* (1983 in press).
- "Elemental Composition of Solar Energetic Particles," W.R. Cook et al., *Ap. J.* **279**, 827-838 (1984).
- "The Voyager Mission: Encounters with Saturn," E.C. Stone, *J. Geophys. Res.* **88**, 8369 (1983).
- "Voyager Measurements of the Energy Spectrum, Charge Composition, and Long Term Temporal Variations of the Anomalous Components in 1977-1982," W. R. Webber and A. C. Cummings, *Proceedings of Solar Wind V Conference, NASA CP 2280*, 427-434 (1983).
- "Temporal Variations of the Anomalous Oxygen Component," A. C. Cummings and W. R. Webber, *Proceedings of Solar Wind V Conference, NASA CP 2280*, 435-440 (1983).
- "Energetic Oxygen and Sulfur Ions in the Jovian Magnetosphere and their Contributions to the Auroral Excitation," N. Gehrels and E.C. Stone, *Proceedings of 5th Conf. on the Physics of the Jovian and Saturnian Magnetospheres* (1983).
- "Elemental Composition of Solar Energetic Particles," H. Breneman et al., *Proceedings of 18th International Cosmic Ray Conference, Bangalore, India* **4**, 35 (1983).

The following is a summary of one of the studies.

### **Studies of Low Energy Cosmic Rays - The Anomalous Component**

The origin of the anomalous component of low energy cosmic rays, of which He and O are the most obvious examples, presents many intriguing questions, such as where and how these particles are accelerated, what their accelerated spectrum looks like, and what their charge state is. One possibility is that they are normal, fully-ionized particles, presumably arriving from outside the solar system. The other is that they are singly charged particles accelerated in the solar system from local interstellar neutrals penetrating the solar system. This latter model provides a natural explanation for why only particles with first ionization potentials  $\geq 13.6$  eV are observed to be anomalous. To address these possibilities, we have analyzed data from the Voyager spacecraft to determine the spectra of anomalous He, N, O, and Ne. We find that the shapes of the spectra are just what one would expect from "conventional" modulation theory (i.e., no drifts) if the spectra of the various anomalous species at the modulation boundary are all power-laws in kinetic energy with approximately the same index and if the particles are *singly ionized*. If the particles are fully ionized, unmodulated spectra that are *very steep* (e.g.,  $\sim E^{-16}$  for O) and *very different* for the different anomalous species (e.g.,  $\sim E^{-8}$  for He) are required.

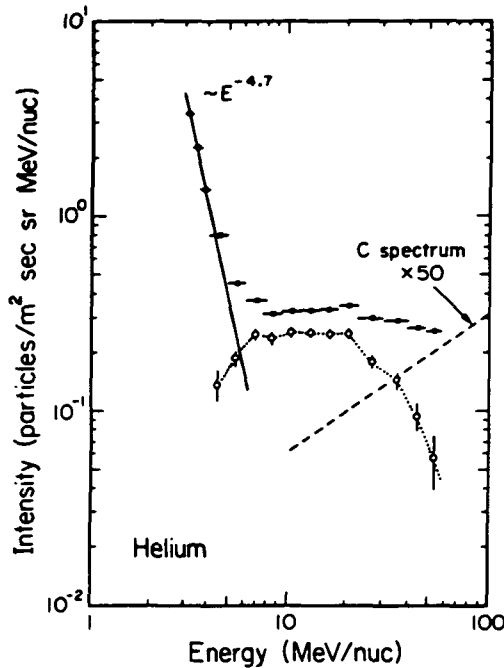


Figure 14

In this analysis individual spectra are obtained for He, C, N, O, and Ne nuclei for a 90 day quiet period between September 1977 and February 1978. During this time period the Voyager spacecraft were between  $\sim 1$  and 2.5 AU and the cosmic ray intensity was at sunspot minimum modulation conditions.

The composite spectrum for He nuclei is shown in Fig. 14 and those for other nuclei in Figs. 15a, b, c, and d. It is to be noted that despite a stringent quiet-time selection criterion a turn-up exists in the low energy He and C spectra, presumably a low level solar or interplanetary component with a He spectrum proportional to  $E^{-4.7}$ . The solid lines in Fig. 15 are scaled from He assuming a charge composition similar to that for corotating events. There is excellent agreement with the C data, suggesting that this low energy turn-up is of solar/interplanetary origin. The dashed lines in Figs. 14 and 15 show the estimated spectra of galactic cosmic rays scaled from the observed high-energy C spectrum. Note that for C the subtraction of the solar/interplanetary component leaves a spectrum (open circles) consistent with a modulated galactic component with no evidence of an anomalous component.

The spectrum of anomalous He shows a peak in the 10-20 MeV/nuc region. The anomalous N and O spectra have regions with small slope, suggestive of a peak in the spectra near 5 MeV/nuc. Although the Ne spectrum is statistically less well-determined, there is no evidence for a peak down to 4 MeV/nuc. We will now show how these differences in peak locations provide information on the origin and charge state of the anomalous component.

Cosmic ray spectra observed near Earth, such as those shown in Figs. 14 and 15, are determined both by the spectra at the boundary of the modulation region and by interplanetary propagation conditions. Recently, Fisk [private communication] has suggested that if the input spectra at the modulation boundary are similar, then characteristic spectral features observed near Earth, such as spectral peaks, should occur at an energy for each species for which the particles have the same interplanetary diffusion coefficient  $\kappa$ . In general,  $\kappa \sim \beta R^7$ , where  $\beta$  is the particle velocity

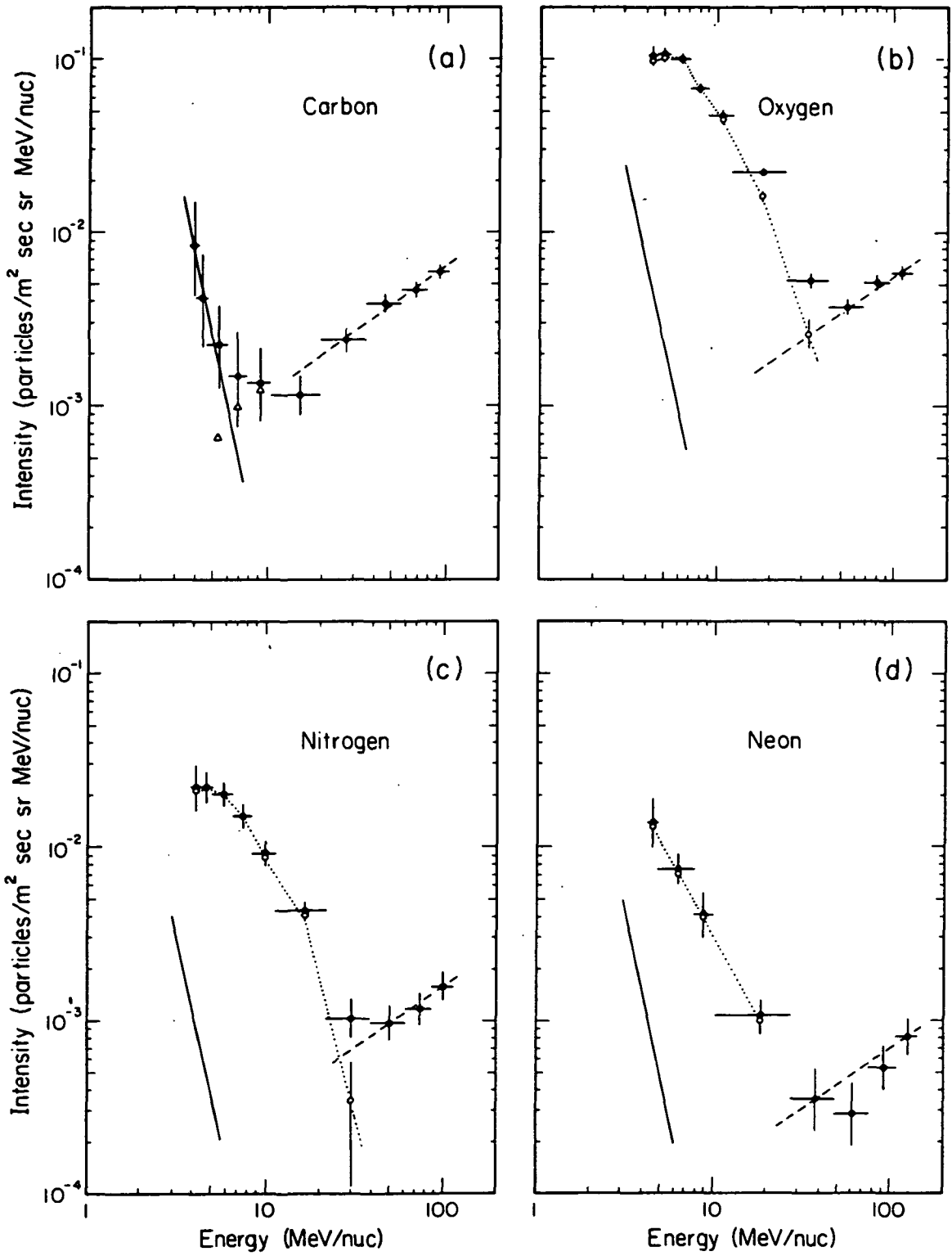


Figure 15

and  $R$  is rigidity. For non-relativistic particles, with energy  $E$  in MeV/nuc,  $R \sim AE^{\kappa}/Z$  and  $\beta \sim E^{\gamma}$ , so that  $\kappa \sim (A/Z)^{\gamma} E^{(\gamma+1)/2}$ . Thus for a given value of  $\kappa$ , the corresponding particle energies scale as

$$f_E(Z,A) \sim (A/Z)^{-2\gamma/(\gamma+1)} \quad (1)$$

For fully-ionized particles with  $A/Z=2$ , the energy scaling factor  $f_E$  is independent of  $Z$  and the location of the peaks in the spectra should occur at the same value of energy/nucleon, as is observed for several galactic cosmic ray nuclei such as C, O, Ne, Mg, and Si but not for the anomalous species shown in Figs. 14 and 15. For singly-ionized particles ( $Z=1$  in equation 1),  $f_E \sim A^{-2\gamma/(\gamma+1)}$  and the spectra should peak at different energies for particles with different  $A$ .

The spectra of Figs. 14 and 15 do not show well-defined peaks for which an energy scaling factor could be accurately derived. However, using numerical solutions to the modulation equation, we find that for boundary spectra which are power-laws in kinetic energy with the same index, not only do the peaks of the modulated spectra scale as indicated by equation 1 but also the *entire spectra* scale as well. This result suggests that the measured spectrum of O when scaled by an appropriate factor ( $f_E$ ) would match that of He. In order to empirically determine these energy scaling factors for the anomalous component, we used the anomalous O spectrum as the reference spectrum (dotted line in Fig. 15b) and scaled the other spectra in energy and intensity to obtain the best fit to it. The values of the energy scaling factors which minimized the  $\chi^2$  of the fit between the spectra are shown in Fig. 16. The one sigma uncertainties correspond to values of  $f_E(Z,A)$  which gave  $\chi^2 = (\chi^2)_{\min} + 1$ . The solid lines in Fig. 16 show the dependence of  $f_E$  on  $A$  for various values of  $\gamma$ , assuming  $Z=1$ . The dashed line at  $f_E = 1$  indicates the mass-independent scaling factor for fully-ionized particles.

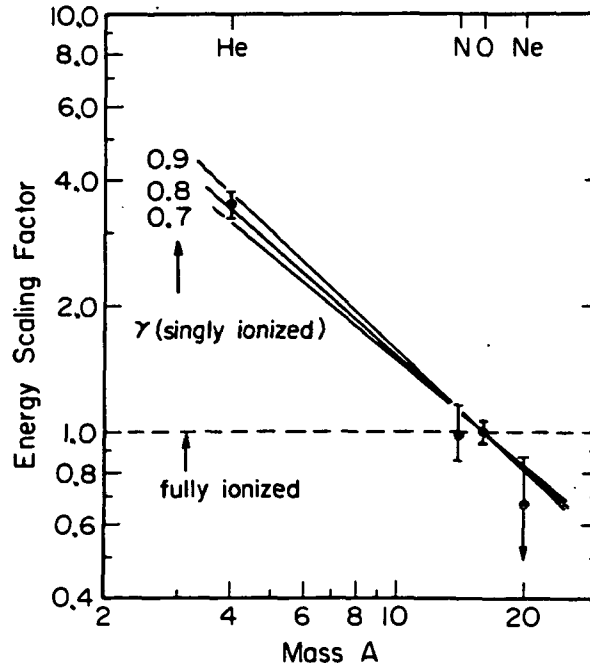


Figure 16

It is clear from Fig. 16 that the observed mass dependence of  $f_E$  is inconsistent with an assumption that the particles are fully ionized. On the other hand, if the particles are assumed to be singly ionized then the mass dependence of the scaling factor is consistent with  $\gamma \approx 0.7-0.9$ . This value is consistent with results from solar particle and interplanetary radial gradient studies.

Similar considerations should apply to the modulation of galactic cosmic rays of different  $A/Z$ . The peak in the spectrum of hydrogen ( $A/Z=1$ ) would be expected to occur at an energy which is a factor of  $\sim 1.85$  larger than the corresponding peak energy/nuc of the helium ( $A/Z=2$ ) spectrum (for  $\gamma=0.8$ ) if the unmodulated spectra were power-laws in kinetic energy of the same index. Measurements of these spectra at the same time in 1977-78 [Webber and Yushak] yields a ratio of  $\sim 1.5$ . This difference indicates that the unmodulated spectra of the galactic component are probably not simple power-laws in kinetic energy. In fact, our numerical studies indicate that by using unmodulated spectra of galactic He and H  $\sim (E+400)^{-2.65}$  and by using a galactic electron spectrum derived from the interstellar radio data, reasonable fits can be made to the 1977 spectra of H, He, and electrons using the same diffusion coefficient as in the anomalous component study.

It is, of course, possible to produce arbitrary peak locations for the anomalous cosmic ray particles, whether singly or fully ionized, if the unmodulated spectra are not constrained to be similar for the different charges. Our numerical studies indicate, for example, that an unmodulated spectrum of fully-ionized O  $\sim E^{-16}$  and of fully-ionized He  $\sim E^{-8}$  could account for the observed near-Earth spectra. For O, such a spectrum results in a modulation factor at  $\sim 5$  MeV/nuc of  $\sim 10^{18}$ . If present throughout the galaxy, the flux of O in the 5-30 MeV/nuc energy interval alone would greatly exceed (by factor of  $\sim 10^{14}$ !) that allowed from considerations of the ionization state of trace elements in the interstellar gas [Fisk]. It would also imply an energy density for 5-30 MeV/nuc O which exceeds that expected for all cosmic rays ( $\sim 1$  eV  $\text{cm}^{-3}$ ) by a factor of  $\sim 10^8$ ! We are suggesting, on the other hand, that a simple model in which the anomalous component is *singly ionized* can account for the observed spectral features of both the galactic and anomalous components when more reasonable forms of the unmodulated spectra are used.

### 1.2.3. A Heavy Isotope Spectrometer Telescope (HIST) Launched on ISEE-3 in August 1978

HIST is designed to measure the isotope abundances and energy spectra of solar and galactic cosmic rays for all elements from lithium to nickel ( $3 \leq Z \leq 28$ ) over an energy range from several MeV/nucleon to several hundred MeV/nucleon. Such measurements are of importance to the study of the isotopic constitution of solar matter and of cosmic ray sources, the study of nucleosynthesis, questions of solar-system origin, studies of acceleration processes and studies of the life history of cosmic rays in the galaxy.

HIST was successfully launched on ISEE-3 and provided high resolution measurements of solar and galactic cosmic ray isotopes until December 1978, when a component failure reduced its isotope resolution capability. Since that time, the instrument has been operating as an element spectrometer for solar flare and interplanetary particle studies.

Our work on solar flare, interplanetary, and galactic cosmic ray isotopes has resulted in the following recent papers.

- "The Elemental and Isotopic Composition of Galactic Cosmic Ray Nuclei," R. A. Mewaldt, *Rev. Geophys. Space Phys.* **21**, 295-305 (1983).
- "Further Isotopic Studies of Heavy Nuclei in the 9/23/78 Solar Flare," R. A. Mewaldt et al., *Proceedings of 18th International Cosmic Ray Conference, Bangalore, India* **4**, 42-45 (1983).

- "A High Resolution Study of the Isotopes of Solar Flare Nuclei," R.A. Mewaldt et al., *Ap. J.* (1984 in press).
- "An Accelerator Test of Semi-Empirical Cross-Sections," K.H. Lau et al., *Proceedings of 18th International Cosmic Ray Conference, Bangalore, India* (1983 in press).
- "The Isotopic Composition of the Anomalous Low-Energy Cosmic Rays," R.A. Mewaldt et al., *Ap. J.* (1983 Submitted).

The results of a joint ISEE/IMP study of the isotopic composition of the anomalous cosmic ray component are summarized below.

### **The Isotopic Composition of the Anomalous Low-Energy Cosmic Rays**

Observations of low-energy cosmic rays during the last solar minimum have revealed that below  $\sim 50$  MeV/nucleon the energy spectra and elemental composition of quiet-time cosmic rays undergo a change in character. Specifically, anomalous enhancements were discovered in the energy spectra of the elements helium, nitrogen, oxygen, and neon relative to other elements such as hydrogen, boron, and carbon. We have made new observations of the isotopic composition of low-energy He, C, N, O, and Ne nuclei, covering the energy interval from  $\sim 5$  to 30 MeV/nucleon, where the "anomalous cosmic ray" (ACR) fluxes have been observed. Comparing the isotopic composition of the anomalous cosmic rays with that of higher-energy galactic cosmic rays (GCR's), we find that for three of the elements studied (He, N, and Ne) there are significant variations in the isotopic composition at essentially the same energy where the elemental composition changes ( $\sim 30$  to 50 MeV/nucleon), in agreement with earlier studies. Thus, fragmentation products such as  $^3\text{He}$  and  $^{15}\text{N}$  appear to be essentially absent from the anomalous cosmic ray component. In addition, we find a difference between the  $^{22}\text{Ne}/^{20}\text{Ne}$  ratios in the anomalous and galactic cosmic rays suggesting that the nucleosynthesis of these two components has differed. Although statistically limited, our low-energy isotope results are generally consistent with the proposed interstellar-neutral origin for the anomalous cosmic rays. If correct, this model suggests that future measurements of anomalous cosmic rays can be used to analyze the isotopic structure and evolution of the local interstellar medium.

Several possible origins have been suggested for the ACR component. It was first suggested that the ACR's originate in a nearby galactic source of unusual composition. Fisk, Ramaty, and Kozlovsky proposed that the ACR component originates from neutral interstellar particles that penetrate the heliosphere, become singly ionized, and are then accelerated to  $\geq 10$  MeV/nucleon in the interplanetary medium. Later models placed the accelerator at the solar wind termination shock. In these local acceleration models the source composition is dominated by those elements which are relatively abundant in the neutral state in the ISM, resulting in a selective enhancement of those elements with a relatively high first ionization potential (i.e., He, N, O, Ne, and Ar), consistent with the observed ACR composition. Isotope studies are a key to understanding the origin of the ACR component. If the ACR's originate in a nearby galactic source of unusual elemental composition, isotopic anomalies might also be expected. If the ACR's represent interstellar neutral particles that have been ionized and accelerated in the heliosphere, or at its boundary, then isotope studies, made at 1 AU, can actually analyze the present isotopic structure of the local ISM.

The bulk of these new observations were made with the Caltech Heavy Isotope Spectrometer Telescope (HIST) on ISEE-3, during quiet time periods from 8/13/78 to 12/1/78. In order to address the question of whether the ACR isotopic composition differs from that of galactic cosmic rays, we have divided the HIST data into two energy intervals at  $\sim 30$  MeV/nucleon, the energy at which the ACR fluxes of N, O, and Ne begin to dominate over the GCR component. In the resulting mass histograms, shown in Figure 17, the observed mass resolution ranges from  $\sim 0.1$  to 0.23 amu.

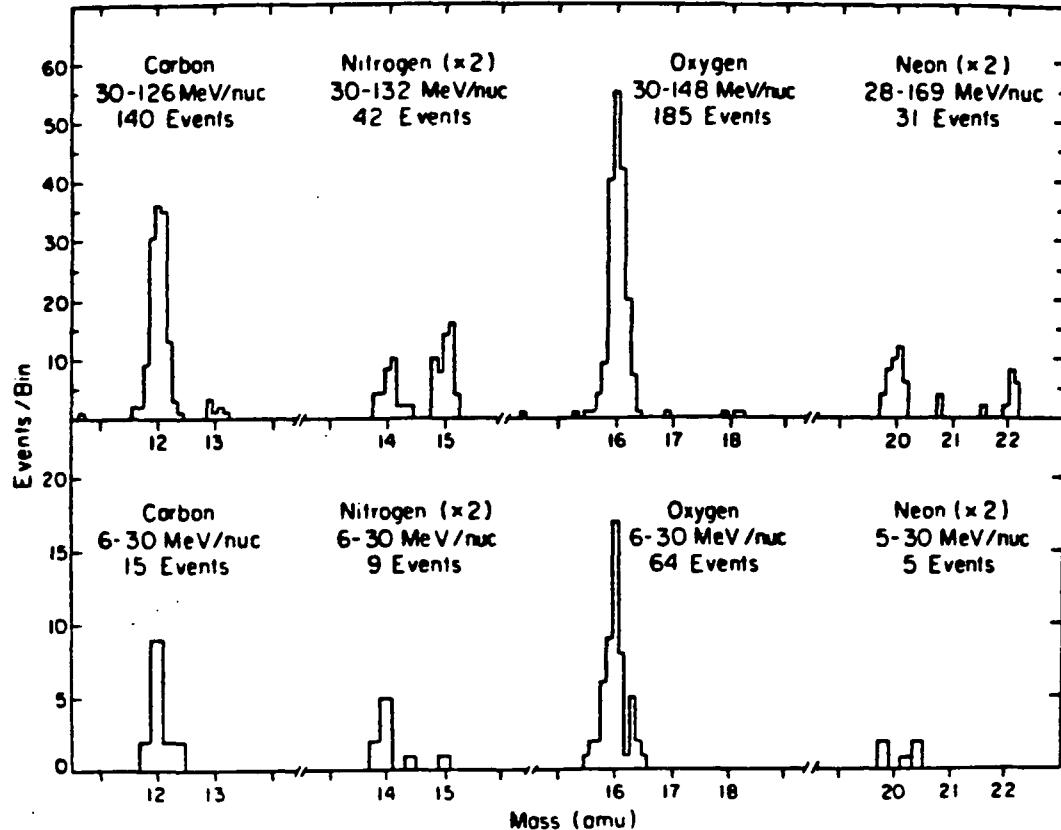


Figure 17

This study also includes IMP-7 isotope data, accumulated during quiet-time periods from October 1972 to June 1978. They represent a continuation of a study first reported in 1975 in which we made the first isotopic measurements of anomalous N and O nuclei. Table 2 summarizes the isotope abundance ratios obtained from the IMP and ISEE data. In Figure 18, these results are compared with selected earlier observations and with the results of GCR propagation and solar modulation calculations.

Comparing the isotope ratios of the GCR component with our low-energy measurements in the region of the ACR component, there are three elements, He, N and Ne, where there are significant differences. In our 1975 study it was already clear that there was significantly less  $^{15}\text{N}$  in the ACR component than in the GCR component. Now, with somewhat better statistical accuracy, we find less than a 0.1% probability that our 6 to 13 MeV/nucleon IMP-7 result is consistent with  $^{15}\text{N}/\text{N} > 0.5$ , as required by the GCR observations. Our ISEE data confirm this ( $^{15}\text{N}/\text{N} < 0.5$  with 99% confidence), as do the recent Voyager data. For  $^{22}\text{Ne}/^{20}\text{Ne}$  we find the 5 to 28 MeV/nucleon ratio to be less than the  $\sim 100$  MeV/nucleon value of  $\sim 0.6$  at the 94% confidence level. This result, and the Voyager measurements at somewhat higher energy, support an earlier suggestion based on Pioneer 10 data, that  $^{22}\text{Ne}$  might be less

Figure 18

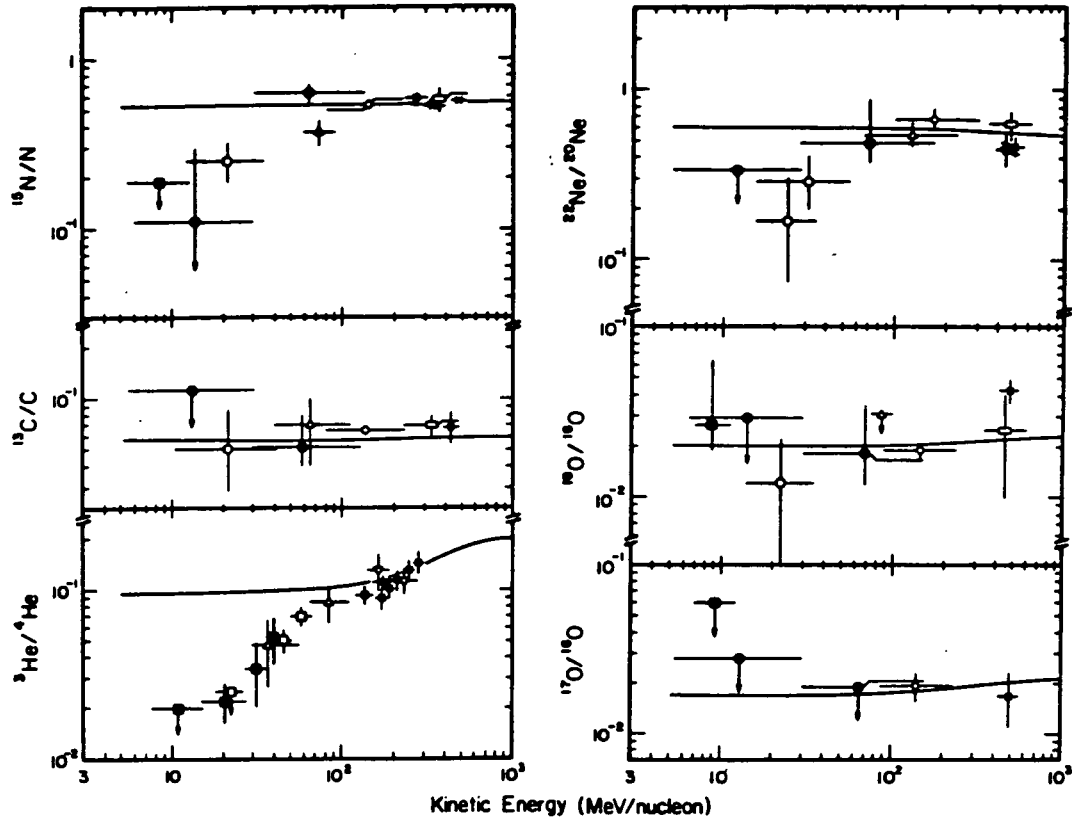


Table 2  
Cosmic Ray Isotope Measurements

Isotope Ratio	Energy (MeV/nuc)	Low Energy Cosmic Rays		Galactic Cosmic Rays (~ 100 MeV/nuc)
		IMP-7 Observed Ratio	ISEE-3 Energy (MeV/nuc) Observed Ratio	
${}^3\text{He}/{}^4\text{He}$	5-15	$\leq 0.02$	—	~ 0.10
${}^{13}\text{C}/\text{C}$	—	—	5-30 $\leq 0.11$	~ 0.06
${}^{15}\text{N}/\text{N}$	6-13	$\leq 0.19$	5-30 $0.11^{+.19}_{-.11}$	~ 0.55
${}^{17}\text{O}/{}^{16}\text{O}$	7-12	$\leq 0.06$	6-30 $\leq 0.03$	~ 0.020
${}^{18}\text{O}/{}^{16}\text{O}$	7-11	$0.03^{+.03}_{-.01}$	6-30 $\leq 0.03$	~ 0.020
${}^{22}\text{Ne}/{}^{20}\text{Ne}$	—	—	5-28 $\leq 0.36$	~ 0.60

abundant at low energies. For the C and O isotopes, the statistical accuracy of the data is not sufficient to determine whether there is an energy dependence to the isotopic composition. Our low energy results do, however, place tighter limits on any possible excess of the rare neutron-rich C and O isotopes at low energies.

To interpret quantitatively the energy dependence of the isotopic composition, we consider a two component description. We assume that the modulated GCR component has a spectral slope  $dJ/dE \propto E^{0.7}$  (consistent with 1 AU measurements) and extrapolate this dependence down to a few MeV/nucleon. For the ACR component, we assume that the elements N, O, and Ne all have the same spectral shape, obtained by subtracting the GCR component from the measured O spectrum and we then consider a range of isotopic compositions in order to deduce the limits imposed by the experimental data. The curves in Figure 19 show the isotopic composition that results from adding the contributions from the two components.

The GCR abundances of  $^{15}\text{N}$  and  $^{18}\text{O}$  are believed to result principally from the fragmentation of heavier cosmic rays as they pass through the ISM. The fact that the ACR  $^{15}\text{N}/\text{N}$  ratio is much lower than the GCR ratio implies that fragmentation contributions are much less important for this component, as is also evidenced by corresponding low-energy decreases in, e.g.  $^3\text{He}/^4\text{He}$  (see Figure 18) and B/O. It can be seen that our IMP  $^{18}\text{O}/^{16}\text{O}$  ratio (based on two  $^{18}\text{O}$  events) is consistent with the GCR ratio, and does not show the low energy decrease observed for  $^{15}\text{N}/\text{N}$ ,  $^3\text{He}/^4\text{He}$ , and B/O. If verified by other measurements (our ISEE data show only that  $^{17}\text{O}/^{16}\text{O}$  and  $^{18}\text{O}/^{16}\text{O}$  are less than 0.03 for the ACR's) this  $^{18}\text{O}$  result would be surprising, since there is little  $^{18}\text{O}$  observed in the ISM, and GCR  $^{18}\text{O}$  is mainly of secondary origin.

The isotope abundance ratio  $^{22}\text{Ne}/^{20}\text{Ne}$  is especially interesting because it takes on a range of values in various samples of matter observed in the solar system. The two most likely possibilities for the composition of the Sun appear to be solar-wind Ne, with  $^{22}\text{Ne}/^{20}\text{Ne} = 0.073$ , and neon-A, a meteoritic component with  $^{22}\text{Ne}/^{20}\text{Ne} = 0.12$ . The isotopic composition of GCR Ne is distinctly different from any of the observed solar system components. Our upper limit for the ACR  $^{22}\text{Ne}/^{20}\text{Ne}$  ratio is lower than both the observed ( $^{22}\text{Ne}/^{20}\text{Ne} \approx 0.6$ ) and the source ( $^{22}\text{Ne}/^{20}\text{Ne} \approx 0.43$ ) compositions for GCR Ne (see Figure 19). Integrated over the 5 to 28 MeV/nucleon energy interval, we find only a 10% probability that our measurement could be consistent with an ACR ratio as large as  $^{22}\text{Ne}/^{20}\text{Ne} = 0.43$ , the best estimate for the GCR-source composition of neon. This suggests that the nucleosynthesis of the ACR and GCR components has differed.

If the model of Fisk, Kozlovsky, and Ramaty is correct, then the nuclei comprising the ACR component represent a sample of the local ISM. The inconsistency between ACR and GCR-source Ne is therefore significant in view of recent models which propose that a majority, if not all, of galactic cosmic rays may represent a sample of the interstellar gas. If both of these components do in fact represent samples of ISM material, then these results indicate that the local ISM differs from that of which the galactic cosmic rays are a sample. It is important to get an improved measurement of ACR Ne isotopes to see if the relative abundances are consistent with any of the observed solar system components such as neon-A or solar-wind Ne.

In summary, we have found further evidence for an energy-dependent isotopic composition at low energies, thereby placing new restrictions on the composition and origin of the ACR component. We find no strong evidence for an exotic isotopic composition; indeed, with the possible exception of  $^{18}\text{O}/^{16}\text{O}$ , our ACR results are entirely consistent with tabulated solar-system abundances, and with the interstellar-neutral origin, in which the ACR's represent a sample of the local ISM. Galactic evolution models predict that the isotopic composition of the ISM should evolve with time as a result of the cumulative effect of nucleosynthesis in successive generations of stars. Although the isotopic composition of Ne in the local ISM is unknown, the isotopic

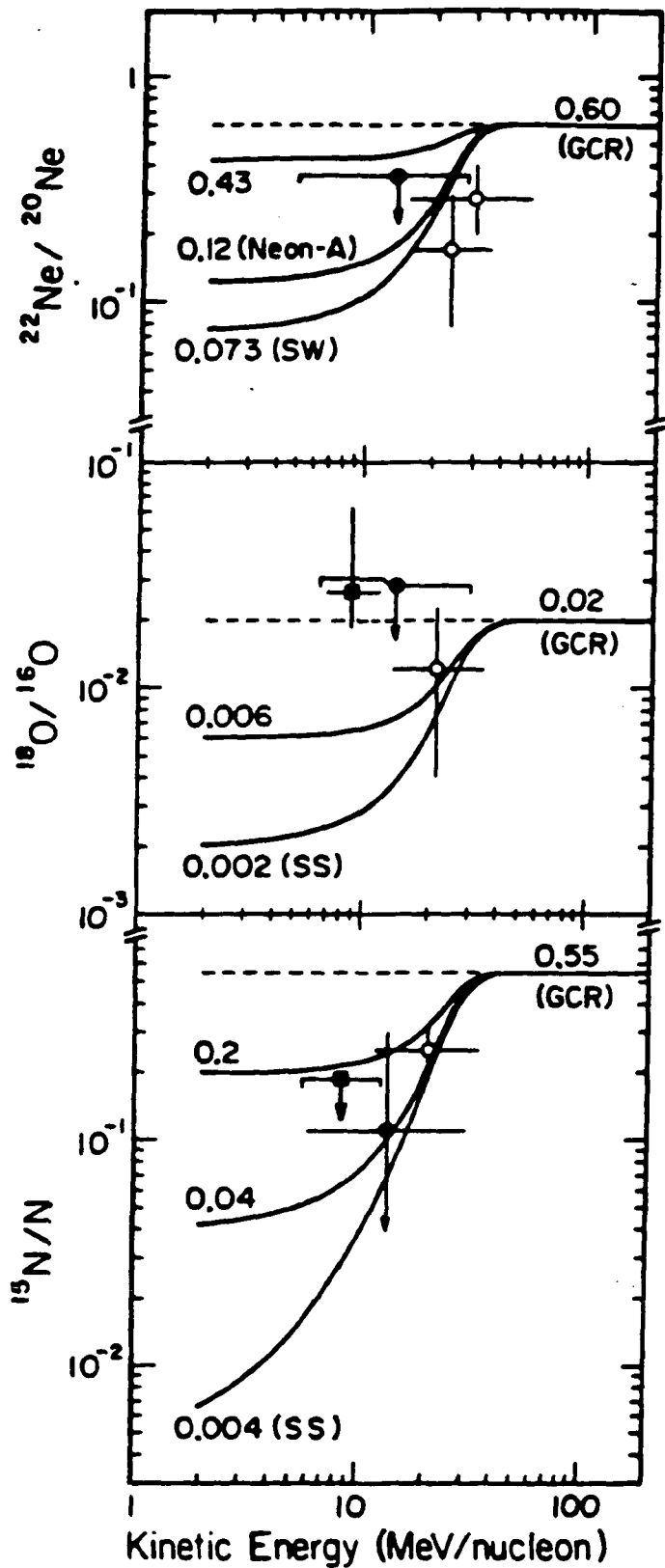


Figure 19

composition of C, N, O, and other elements has been measured in the ISM by radio astronomy studies of interstellar molecules. While such measurements indicate important differences between the interstellar gas and the solar system isotopic abundances, these differences are of the order of a factor of two or three, and would not be detectable with the present ACR isotope measurements. However, if measurements with mass resolution comparable to that from our ISEE experiment could be obtained over a several-year period, isotopic variations of the magnitude observed for N and O isotopes in the ISM should be detectable in the ACR component at energies below  $\sim 10$  MeV/nucleon. Thus, future measurements of this kind, possibly during the next solar minimum period, may provide a unique opportunity to study the evolution of the ISM in the solar neighborhood.

#### 1.2.4. A Heavy Nuclei Experiment (HNE) Launched on HEAO-C in September 1979

The Heavy Nuclei Experiment is a joint experiment involving this group and M. H. Israel, J. Klarmann, W. R. Binns (Washington University) and C. J. Waddington (University of Minnesota). HNE is designed to measure the elemental abundances of relativistic high-Z cosmic ray nuclei ( $17 \leq Z \leq 130$ ). The results of such measurements are of significance to the studies of nucleosynthesis and stellar structures, the existence of extreme transuranic nuclei, the origin of cosmic rays, and the physical properties of the interstellar medium. HNE was successfully launched on HEAO-3 and operated until gyro failure in late May 1981.

Eight papers were presented at the 18th International Cosmic Ray Conference in Bangalore, India reporting results of the calibration at the Lawrence Berkeley Lab Bevalac and flight results based on improved data analysis techniques.

- "Cosmic Ray Elemental Abundances for  $26 \leq Z \leq 42$  Measured on HEAO-3," W.R. Binns et al., *Proceedings of 18th International Cosmic Ray Conference, Bangalore, India* (1983 in press).
- "Cosmic-Ray Abundances of the Even Charge Elements from  $^{50}\text{Sn}$  to  $^{58}\text{Ce}$  Measured on HEAO-3," E.C. Stone et al., *Proceedings of 18th International Cosmic Ray Conference, Bangalore, India* (1983 in press).
- "The Cosmic-Ray Abundances of the Platinum-Lead Elements as Measured on HEAO-3," D.J. Fixsen et al., *Proceedings of 18th International Cosmic Ray Conference, Bangalore, India* (1983 in press).
- "Energy Spectra of Ultraheavy Cosmic Rays Results from HEAO-3," M.H. Israel et al., *Proceedings of 18th International Cosmic Ray Conference, Bangalore, India* (1983 in press).
- "Interactions of 200 GeV Gold Nuclei in Light Elements," N.R. Brewster et al., *Proceedings of 18th International Cosmic Ray Conference, Bangalore, India* (1983 in press).
- "Abundances of 'Secondary' Elements Among the Ultraheavy Cosmic Rays - Results from HEAO-3," J. Klarmann et al., *Proceedings of 18th International Cosmic Ray Conference, Bangalore, India* (1983 in press).
- "Correlation of Source Abundances of Ultraheavy Cosmic Rays with First Ionization Potential - Results from HEAO-3," M.H. Israel et al., *Proceedings of 18th International Cosmic Ray Conference, Bangalore, India* (1983 in press).

- "The Non- $Z^2$  Response of the Heavy Nuclei Cosmic Ray Detector on HEAO-3," T.L. Garrard et al., *Proceedings of 18th International Cosmic Ray Conference, Bangalore, India* (1983 in press).

In addition the following talks and papers have been presented and a thesis completed:

- "The Non- $Z^2$  Response of the Heavy Nuclei Cosmic-Ray Detector on HEAO-3," B.J. Newport et al., *Bull. Am. Phys. Soc.* **28**, 755 (1983).
- "Interactions of 200 GeV Gold Nuclei," N.R. Brewster et al., *Bull. Am. Phys. Soc.* **28**, 755 (1983).
- "The Relative Abundances of Sn, Te, Xe, Ba, and Ce in the Cosmic Radiation," K. Krombel, *Ph.D. Thesis, CIT* (1983).

We report below our observations on those elements in the platinum-lead region.

### Cosmic Ray Abundances of the Platinum-Lead Elements

A primary objective of these studies is to compare the abundances in the source of cosmic rays with those predicted by models of nucleosynthesis. In this charge range most of the nuclides are synthesized by either the rapid (r-process) or slow (s-process) addition of neutrons to lighter seed nuclei. Thus measured abundances, such as that characteristic of solar system (SS) material, or galactic cosmic ray source material may be interpreted as a mix of r- and s-process nuclides. The lead-platinum region provides a sensitive test of the mix of the cosmic ray source abundances, since "platinum" (actually  ${}_{76}\text{Os}$ - ${}_{78}\text{Pt}$ ) is almost exclusively produced by the r-process, while "lead" is a product of both the r- and s-process. An observed ratio of Pb to Pt, here defined as  $R = (80 \leq Z \leq 83) / (75 \leq Z \leq 79)$ , can be compared with values calculated for a particular source abundance and propagation model.

Our charge spectrum is given in Fig. 20, which shows the actual numbers of measured particles. These abundances have been normalized to  $(17.4 \pm 1.0) \times 10^6$  iron nuclei (in the detector). They can be approximately corrected to near earth space by an 11% correction for losses due to interactions within the detector and by 9% and 4% corrections to the "Pb" and "Pt" due to propagation through the Al front window.

Table 3 shows predicted values of R for various source models, and the observed value. The "Detector" values have been corrected for the effects of window material. The calculations use the propagation codes of Brewster et al., with and without allowance for the effects of first ionization potentials (FIP). It can be seen that for this propagation model, the differences in R between r- and SS-like material are significant and generally measurable. In these predictions we have used the solar system abundances of Anders and Ebihara and two versions of r-process abundances, that calculated by us (r1) from a s-process deconvolution of the solar system abundances of Cameron and one deduced by Cameron (r2). The important difference between them is in the derived abundances of lead.

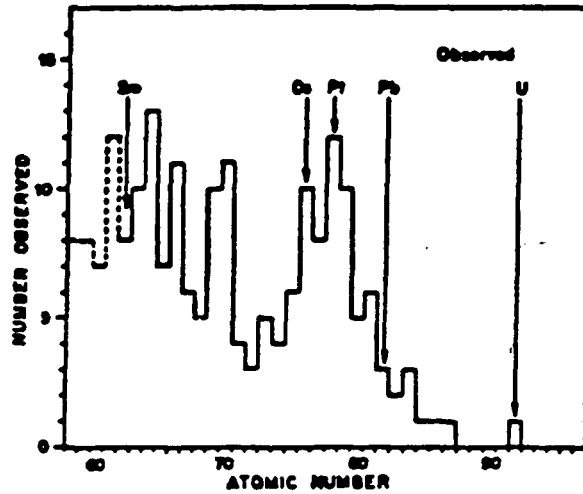


Figure 20

Table 3  
Abundance ratios predicted and observed for various source spectra

Source Type	Source	R Near Earth	R Detector
SS	1.34	1.08	1.05
SS(FIP)	1.93	1.48	1.42
r1	0.047	0.044	0.042
r1(FIP)	0.052	0.049	0.048
r2	0.47	0.42	0.41
r2(FIP)	0.72	0.63	0.62

Observed Number                      22/46                      Ratio  $0.42 \pm 0.18$

The cosmic ray abundances appear to be depleted in lead when compared with the solar system by a factor of at least two to three. Similarly we also found (83 status report) that in the Sn-Ce region (50 to 58 in Z) the ratio of r-process to s-process contribution to the cosmic ray source abundances (taking account of FIP effects) is larger than the corresponding ratio in the solar system.

Noting that Pb is one of the few volatile elements with low FIP, one might interpret the Pb depletion by arguing that volatility rather than FIP is the organizing parameter for cosmic ray source depletion. An underabundance of lead would then be expected, while there would be a smaller effect in the Sn-Ce region, since although Sn like Pb is a low FIP volatile s-process element, the s-process in that region is not only determined by Sn. In this interpretation it may not be necessary to require any unusual ratios of r- and s-process abundances.

An alternative interpretation of these two results is that both indicate an s-process depletion which implies that the source composition is measurably different from that of solar system material.

### 1.2.5. A Magnetometer Experiment on Pioneer 11

The Pioneer 11 Vector Helium Magnetometer Experiment is a joint investigation involving several research centers, with E. J. Smith (JPL) as principal investigator. Leverett Davis, Jr. (SRL) is the Caltech co-investigator on the experiment.

The reanalysis of the magnetometer data for Saturn's field inside  $8 R_s$  was continued and significant improvements in the fit of the models were achieved. Studies of the residuals of a model that fit well indicated that the external field had changed during the encounter and that different values of  $G_1^0$  should be used on the inbound and outbound parts of the encounter. This made a significant improvement in the fit, changing the weighted root mean square percent residual from 1.85% to 1.63%. Connerney, Acuna, and Ness found that their  $Z_3$  model would better fit the Pioneer 11 data if the measured magnetic field were rotated 1.4degree about the spin axis of the Pioneer 11 spacecraft. Davis thereupon included roll correction parameters in his analyses and found that while his weighted root mean square residual percent residual for the  $Z_3$  model with a 1.4degree roll was 2.01%, the corresponding residual for his best fit model, which used a 1.1degree roll inbound and a 0.4degree roll outbound and a more reasonable exterior field source model, was 1.12%. The interior source coefficients for this model are reasonable close to, but distinctly different from, those for the  $Z_3$  model. Subsequently it was confirmed by the Imaging Photopolarimeter experimenters on Pioneer 11 that roll corrections were necessary and that while they varied throughout the encounter, they were reasonably close to those deduced by Davis.

These analyses have made it abundantly clear that the external sources due to ring currents, magnetopause currents, tail currents etc. must be carefully modeled with due attention to the possibility that they may change from one encounter to another or even within one encounter. It is very difficult to know if they have been modeled well.

The manuscript for the chapter entitled "Magnetic Field Models" by J. E. P. Connerney, L. Davis, and D. L. Chenette for T. Gehrels' book on Saturn was completed.

### 1.2.6. Proposal for an Advanced Composition Explorer (ACE)

This investigation, proposed jointly by this group, and by W. D. Arnett and J. A. Simpson (University of Chicago), L. F. Burlaga (GSFC), R. E. Gold and S. M. Krimigis (APL/JHU), W. C. Feldman (LANL), G. Gloeckler and G. M. Mason (UMd), and J. V. Hollweg (UNH), is for the study of an Advanced Composition Explorer (ACE). This Explorer-class mission would make comprehensive measurements of the elemental and isotopic composition of accelerated nuclei with increased sensitivity of several orders of magnitude, and with improved mass and charge resolution. ACE would observe particles of solar, interplanetary, and galactic origins, spanning the energy range from that of the solar wind ( $\sim 1$  keV/nucleon) to galactic cosmic ray energies (several hundred MeV/nucleon). Definitive studies would be made of the abundance of essentially all isotopes from H to Zn ( $1 \leq Z \leq 30$ ), with exploratory isotope studies extending to Zr ( $Z=40$ ), and element studies extending to U ( $Z=92$ ).

ACE would be a coordinated experimental and theoretical effort, designed to investigate a wide range of fundamental problems. In particular, ACE would provide the first extensive tabulation of solar *isotopic* abundances based on direct sampling of solar material and would establish the pattern of *isotopic differences* between galactic cosmic ray and solar system matter. These composition data would be used to investigate basic dynamical processes that include the formation of the solar corona, the acceleration of the solar wind, and the acceleration and propagation of

energetic nuclei on the Sun, in interplanetary space, and in cosmic ray sources. They would also be used to study the history of solar system material and of galactic cosmic ray material, and to investigate the differences in their origin and evolution.

The ACE study payload includes four high resolution spectrometers, each designed to provide the ultimate charge and mass resolution in its particular energy range, and each having a collecting power 1 to 3 orders of magnitude greater than previous or planned experiments. Included in the study would be two spectrometers, a Solar Isotope Spectrometer (SIS) and a Cosmic Ray Isotope Spectrometer (CRIS), for which Caltech would play a leading role. These spectrometers would make use of the proven mass-resolution techniques and large-area detectors that were developed and tested by this laboratory over the past decade, partly through the support of this grant.

## 2. Gamma Rays

This research program is directed toward the investigation of galactic and solar gamma rays with spectrometers of high angular resolution and moderate energy resolution carried on spacecraft and balloons. The main efforts of the group, which are supported partially or fully by this grant, have been directed toward the following two categories of experiments.

### 2.1. Activities in Support of or in Preparation for Spacecraft Experiments

These activities generally embrace prototypes of experiments on existing or future NASA spacecraft and they complement and/or support such experiments.

#### 2.1.1. A Balloon-Borne Gamma Ray Imaging Payload (GRIP)

The principal focus of our current gamma-ray astronomy effort is the construction of a balloon-borne imaging gamma-ray telescope for galactic and extragalactic astronomy observations. A shielded NaI Anger camera will be used in combination with a lead rotating coded aperture mask to achieve an imaging capability of 1000  $0.6^\circ$  pixels in a  $20^\circ$  field of view and a localization capability of 3 arc minutes for  $10\sigma$  sources. This performance represents more than an order of magnitude improvement over previous balloon and satellite instrumentation. The 40 cm x 5 cm NaI Anger camera plate will have an energy range from 30 keV to 3 MeV and achieve a continuum sensitivity of  $1 \times 10^{-6} / \text{cm}^2 \text{ s keV}$  at 1 MeV.

Figure 21 shows a drawing of the detector and coded aperture mask systems of the GRIP instrument. The table lists the key parameters of the instrument.

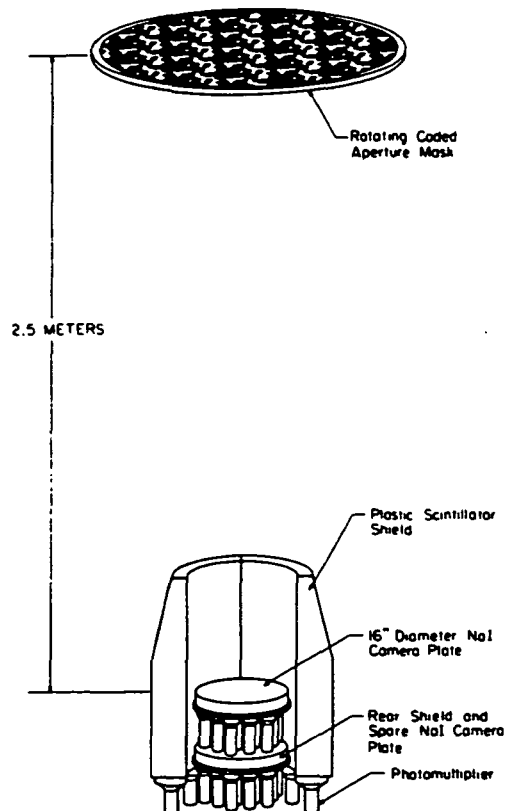


Figure 21

<b>GRIP Balloon Telescope</b>	
<b>Primary Detector</b>	40 cm x 5 cm NaI Anger Camera Position Resolution: 5 mm FWHM @ 200 keV
<b>Shield</b>	Back Plate: 5 cm NaI Side: 16 cm plastic scintillator
<b>Mask</b>	Hexagonal URA: 1.1 m diameter x 2 cm Pb Rotation rate: 1 rpm Spacing: 2.5 m from NaI detector No. of Cells: 1750 (2.5 cm)
<b>Energy Range</b>	0.03 - 3 MeV
<b>Energy Resolution</b>	8.3 keV @ 50 keV; 78 keV @ 1 MeV
<b>Sensitivity (3<math>\sigma</math> - 8 hr) (Southern Hemisphere)</b>	Continuum: ( $\Delta E/E = 1$ ) @ 100 keV - $1 \times 10^{-5}$ ph/cm <sup>2</sup> s keV @ 1 MeV - $1 \times 10^{-6}$ ph/cm <sup>2</sup> s keV Broad Line: ( $\Delta E/E = 1.2 \times$ FWHM resolution) $\sim 3 \times 10^{-4}$ ph/cm <sup>2</sup> s: 100 keV - 1 MeV
<b>Imaging</b>	Resolution: 1000 0.6° diameter pixels (20° FOV) Angular localization: 3 arc min (10 $\sigma$ source)

Considerable progress has been made during the last year in all principal hardware areas:

• **Primary Detector & Shield**

NaI Anger Cameras - Primary unit completely assembled and mapped.  
Components for backup unit fabricated and assembled.  
Plastic shield segments - Shield segments tested for light output and position response. All segments wrapped. PMT's tested and bases partially assembled.

• **Flight Electronics and Support Systems**

ADC's: High rate with excellent linearity - derived from HEIST cosmic ray experiment design. Required 20 ADC's fabricated and tested.  
 $\mu$ P - Control and pointing  $\mu$ P's functioning with FORTH operating system. Communication and control link established with PDP 11/24 GSE running UNIX.  
VCR's: 10 VCR's procured. Digital encoding using commercial audio digitizer allows virtually error-free recording at 1.4 Mb/s.

• **Telescope Enclosure**

Camera plate and shield support fixture fabricated.  
Telescope shell and domes under fabrication.  
Mask tower fabricated.  
Mask rotator and position encoder under fabrication.

• **Pointing System (Development Supported by Caltech Funds)**

Pointing platform design and stress analysis in progress.  
Azimuthal torquer and universal joint under fabrication.  
Support electronics equipment box and radiative cooler designed.  
Rate gyroscope vendor selection in progress.

The design of the instrument is based on earlier laboratory investigations of imaging with rotating hexagonally symmetric coded aperture masks. This technique was described in the following paper:

- "Gamma-Ray Imaging with a Rotating Hexagonal Uniformly Redundant Array." W. R. Cook et al., *IEEE Trans. Nuclear Sci.* NS-31, 771-775 (1984).

### 2.1.2. Development of Large Anger Camera Detectors for $\gamma$ -ray Astronomy

The GRIP instrument employs a 40 cm diameter, 5 cm thick NaI crystal as its primary detector. The NaI scintillator is configured in the "Anger camera" mode, that is, the photomultiplier tubes (PMT's) are individually pulse height analyzed to determine the  $\gamma$ -ray interaction position using the ratio of signals in the PMT's.

Conventional Anger cameras such as those used in nuclear medicine are relatively thin (typically 1.25 cm) and limited to energies below 200 keV. Position determination in these detector is relatively straightforward. The interaction position is essentially the signal weighted vector sum of the PMT positions.

Because we wish to extend the response of the GRIP balloon instrument to 1 MeV and above, a considerably thicker detector is needed. A 5 cm thick detector has a photopeak efficiency of 38% at 1 MeV compared to 6% for a 1.25 cm thick detector. However, analysis of the signals from a thick detector is considerably more complicated. The complication arises from two sources: first, edge effects are more important in the thick detector because of the increased ratio of thickness to diameter; and second, there is a dependence of the PMT signals on the depth of the interaction position in the detector. Consequently, the position determination algorithm must be three dimensional in nature, treating the depth ( $z$ ) dependence, as well as the planar ( $x$ - $y$ ) dependence.

We have employed maximum likelihood techniques to obtain a measurement of the event position. Let  $N_i(\mathbf{x})$  be the number of photons expected in PMT  $i$  due to a  $\gamma$ -ray interaction at position  $\mathbf{x}$ . Then the logarithm of the likelihood function can be shown to be:

$$\ln(L) = \sum_i n_i \ln(N_i(\mathbf{x}))$$

where  $n_i$  are the measured photomultiplier tube signals. The measured event position is defined to be that  $\mathbf{x}$  which maximizes the likelihood function. To maximize  $\ln(L)$ , the function  $N_i(\mathbf{x})$  must be determined from calibrations, and this is approximated by:

$$N_i(\mathbf{x}) \approx N_i(\mathbf{x}_0) + \sum_j \frac{dN_i(\mathbf{x}_0)}{dx_j} \Delta x_j$$

where  $\mathbf{x}_0$  denotes the calibration position nearest to  $\mathbf{x}$ ,  $\Delta x_j$  is the  $j$ th component of  $(\mathbf{x} - \mathbf{x}_0)$ , and the  $N_i(\mathbf{x}_0)$  and derivatives are measured mean values at the calibration points. The calibration points were chosen to lie on a grid with 2.35 cm spacing. After the interaction position is determined by the maximum likelihood criterion, distortions are removed by using the cross derivatives of  $N_i(\mathbf{x})$  in  $x$ - $z$  and  $y$ - $z$ .

Figure 22 shows measured event positions obtained from the likelihood analysis. The events were produced by collimated 662 keV  $\gamma$ -rays perpendicularly incident of the Anger camera at a number of grid positions. In actuality, one twelfth of the crystal was mapped, the other segments shown in Figure 22 were obtained from the mapping data by reflection symmetry so that the resolution could be easily related to the scale and shape of the detector.

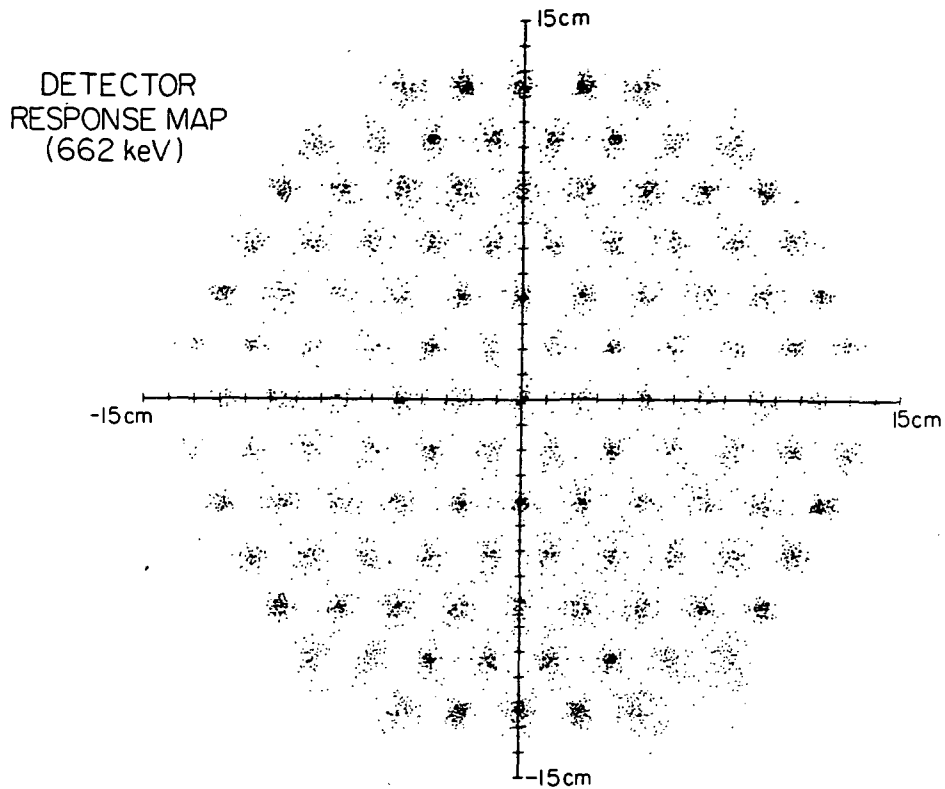


Figure 22

Figure 23 shows the position resolution spread function of the central grid point of Figure 22. The position resolution is 7 mm FWHM in both x and y directions.

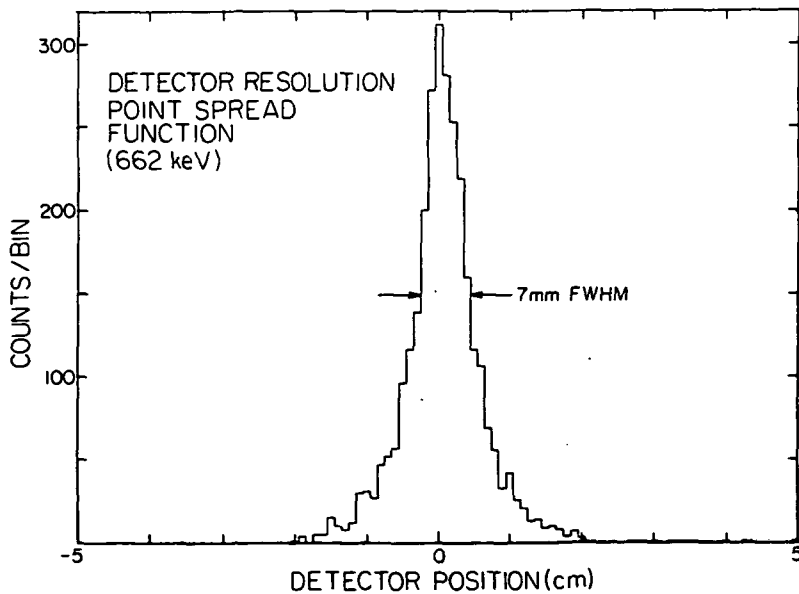


Figure 23

Figure 24 shows a calculation of the expected position resolution as a function of energy. The calculation uses a Monte Carlo  $\gamma$ -ray propagation coded to determine the Compton scattering contribution to the FWHM position resolution for energies between 50 keV and 2 MeV. The curve is normalized to the measured position resolution at 122 keV and gaussian statistics are assumed to determine the contribution of light collection effects to the FWHM position resolution.

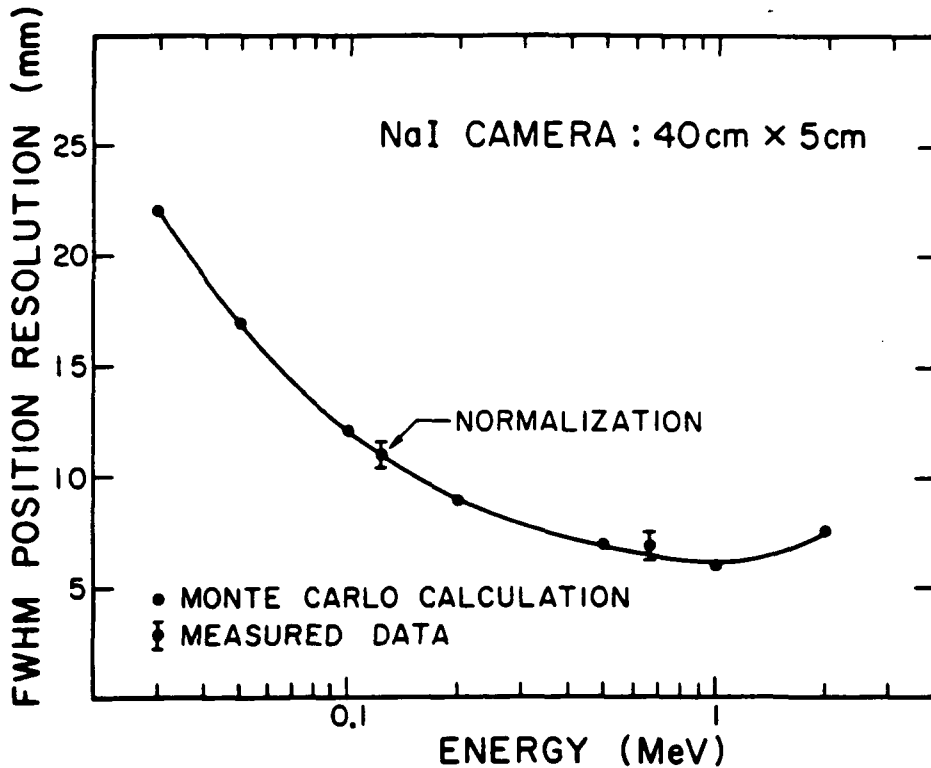


Figure 24

An interesting consequence of the development of a three dimensional position determination algorithm is the capability of measuring the depth of the  $\gamma$ -ray interaction in the detector. This depth determination capability is potentially very useful since it allows the implementation of an "integral shield" which can be used to reject background. For instance, low energy  $\gamma$ -rays are expected to interact primarily near the front face of the crystal. The interaction length for  $\gamma$ -rays of less than 300 keV energy is less than 1.5cm. Thus, events with interaction positions in the back half of the Anger camera can be rejected as background induced events. Furthermore, the rejection criteria can be optimized for the energy of interest since the depth determination is performed ex post facto in the data analysis.

Figure 25 gives an indication of the depth determination capability of the GRIP NaI detector. The detector was flooded from front and back by  $\gamma$ -rays of 122 keV. Figure 25 shows the individual z-position histograms for events incident from the front and back. A depth selection which accepts 90% of the 122 keV  $\gamma$ -rays incident from the front will reject 87% of the  $\gamma$ -rays incident from the back. Alternatively, a depth selection which accepts 90% of the "source" events incident on the front of the NaI detector will reduce a uniform internal background by a factor of two.

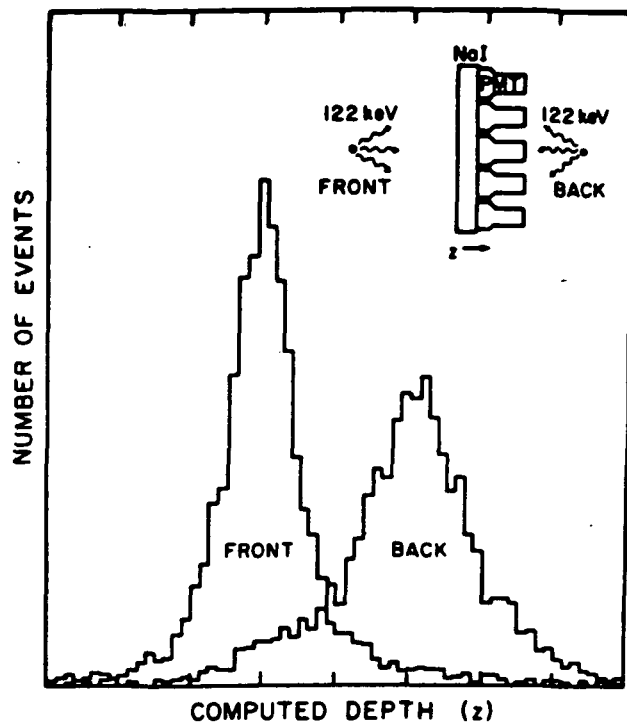


Figure 25

The background rejection provided by the depth selection will improve the sensitivity of the GRIP experiment. The extent of this improvement will depend on the exact spatial distribution of background observed during flight. We note that the on-off background subtraction provided by the rotating mask assures that any spatial non-uniformity in the background rejection will not impact the imaging characteristics of the GRIP telescope as long as the source event detection efficiency is well known.

### 2.1.3. Technology Development

During the time period of this report, we completed the study of mercuric iodide ( $\text{HgI}_2$ ) detectors for potential use in gamma-ray spectrometers. This work was funded in part by the Director's Discretionary Fund of the Jet Propulsion Laboratory. Techniques were developed for enhancing the energy resolution of  $\text{HgI}_2$  detectors, providing energy resolution better than that available from NaI scintillation detectors. Figure 26 shows the energy resolution enhancement obtained through a two-dimensional pulse processing technique. Using conventional techniques the energy resolution was 8.3% at 862 keV with a peak to valley ratio for the full energy peak of 2:1 (Figure 26a). The two-dimensional pulse processing technique improves the energy resolution to 2.6% at 862 keV and the peak to valley ratio is improved to 9:1 (Figure 26b). This work is reported in detail in the following paper:

- "Energy Resolution Enhancement of Mercuric Iodide Detectors," M. Finger et al., *IEEE Transaction on Nuclear Science* NS-31, 348-352 (1984).

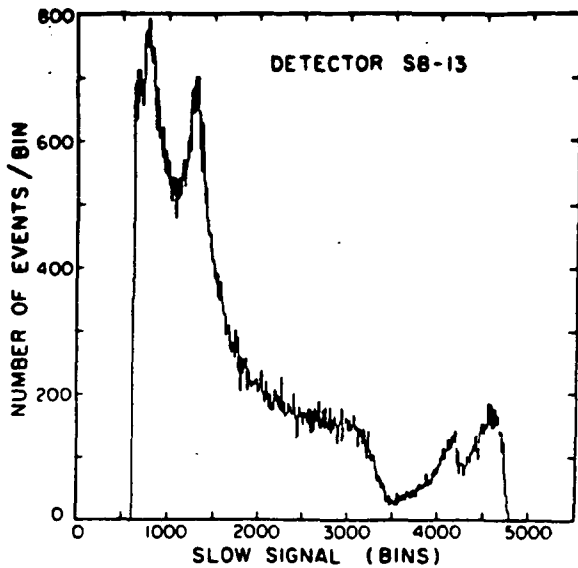


Figure 26a

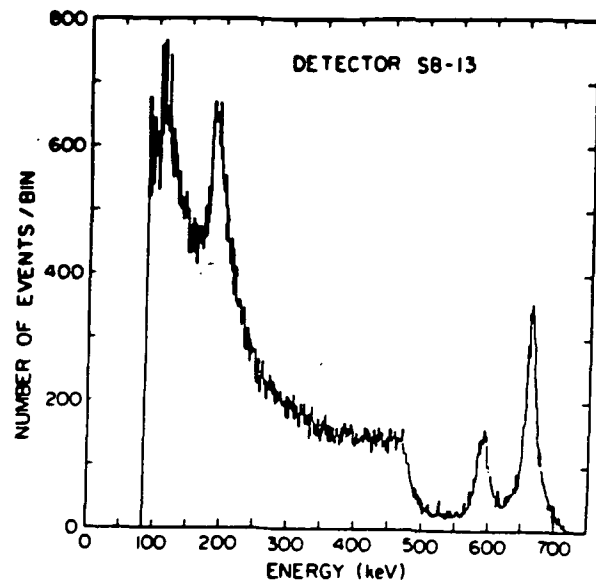


Figure 26b

## 2.2. Experiments on NASA Spacecraft

### 2.2.1. The Gamma Ray Spectrometer Experiment on the Solar Maximum Mission

The Solar Maximum Mission satellite (SMM) was launched in early 1980 and has been in continuous operation observing gamma-ray emission from solar flares. The instrument is sensitive to photons in the energy range 0.3-100 MeV, and can also detect energetic neutrons above 40 MeV.

We have collaborated with the University of New Hampshire in the study of 2.22 MeV emission, following up on our earlier work with the HEAO-3 spacecraft. The focus of the SMM data analysis has been a study of 2.22 MeV line emission in a sample of 8 flares, which includes the very intense solar flare of 3 June 1982. The data from these flares has allowed a detailed study of the time history of the 2.22 MeV neutron capture line from which conclusions have been drawn concerning the production of low energy neutrons in solar flares, the density at which neutrons are captured, and the  $^3\text{He}$  abundance in the photosphere.

Figure 27 shows the time history of the 2.22 MeV emission from the 3 June 1982 flare together with a model for 2.22 MeV emission based on Monte Carlo calculations of neutron propagation in the solar photosphere. The neutron propagation calculation accounts for energetic neutron scattering, thermal diffusion, and neutron capture on  $^3\text{He}$  and  $^1\text{H}$ . A new feature of this particular Monte Carlo calculation is its use of the measured energetic neutron spectrum as input data. The energetic neutron spectrum was determined by three different observations: direct measurements of energetic neutrons at 1 A.U. by the SMM spacecraft, observations with mountain altitude neutron monitors, and neutron decay proton measurements by the ISEE spacecraft. The time production rate of neutrons was taken to be the same as that of 4-8 MeV photons which are tracers of energetic nucleon interactions. The only remaining free parameters of the model are the overall 2.22 MeV photon intensity and the  $^3\text{He}/^1\text{H}$  ratio in the photosphere.

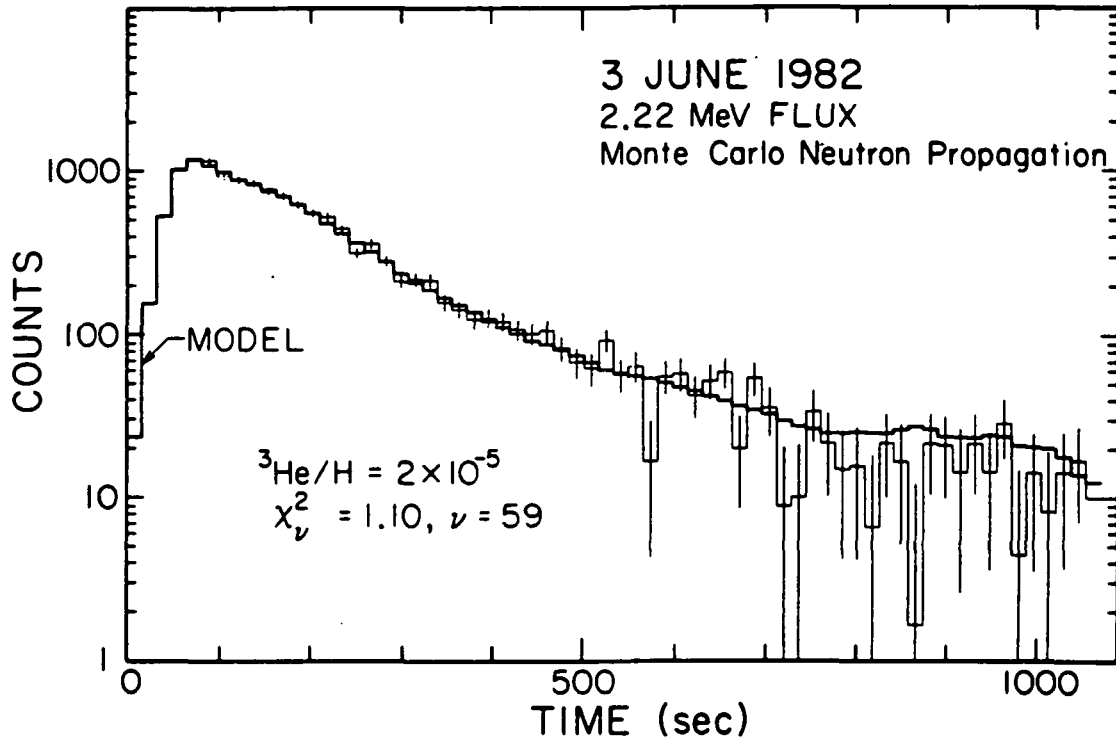


Figure 27

Figure 27 indicates that the calculated model provides an excellent fit to the data for a  ${}^3\text{He}/{}^1\text{H}$  ratio of  $2 \times 10^{-5}$ . The fact that the model fit is quite accurate allows much better quantitative estimates of nuclear interaction rates in solar flares using measurements of the 2.22 MeV intensity. This is significant since the 2.22 MeV line is the most intense line observed in solar flares and thus can provide unambiguous evidence for nucleon acceleration even in weak flares. Using the predictions of the Monte Carlo model, 2.22 MeV line observations from flares other than the 3 June 1982 flare can be corrected for location on the solar disk and for duration of observation to give accurate estimates of the flux of low energy neutrons and flare protons. Preliminary results of this work were reported in the following paper and talk:

- "The Time History of 2.22 MeV Line Emission in Solar Flares," T.A. Prince et al., *Proceedings of 18th International Cosmic Ray Conference*, 4, 79-82 (1983).
- "The Energetic Particle and Photon Component of Solar Flares," T.A. Prince, *Bull. Am. Phys. Soc.* 29, 71 (1983).

### **3. Other Activities**

A. Buffington served as chairman and immediate past chairman of the APS Division of Cosmic Physics.

T. A. Prince has received a Presidential Young Investigator Award from the National Science Foundation.

E. C. Stone continues to serve as NASA's Project Scientist for the Voyager Mission. He is also a member of the Space Science Board, the Solar System Exploration Committee, and the NASA/University Relations Study Group. He is currently a member of the Division for Planetary Sciences Committee of the American Astronomical Society and is a member of the steering group of the Space Sciences Working Group.

#### 4. Bibliography

- "Microstructure of Magnetic Reconnection in Earth's Magnetotail," Bieber, J. W. et al., *J. Geophys. Res.* (submitted for 1984).
- "Cosmic Ray Elemental Abundances for  $26 \leq Z \leq 42$  Measured on HEAO-3," Binns, W.R. et al., *Proceedings of 18th International Cosmic Ray Conference, Bangalore, India* (1983 in press).
- "Elemental Composition of Solar Energetic Particles," Breneman, H. et al., *Proceedings of 18th International Cosmic Ray Conference, Bangalore, India* 4, 35 (1983).
- "Interactions of 200 GeV Gold Nuclei," Brewster, N.R. et al., *Bull. Am. Phys. Soc.* 28, 755 (1983).
- "Interactions of 200 GeV Gold Nuclei in Light Elements," Brewster, N.R. et al., *Proceedings of 18th International Cosmic Ray Conference, Bangalore, India* (1983 in press).
- "Further Analysis of a Recent Cosmic-Ray Antiproton Experiment," Buffington, A. and S. M. Schindler, *Proceedings of 18th International Cosmic Ray Conference, Bangalore, India* 2, 71-74 (1983).
- "A Cerenkov - dE/dX Experiment for Measuring Cosmic-Ray Isotopes from Neon Through Iron," Buffington, A. et al., *Proceedings of 18th International Cosmic Ray Conference, Bangalore, India* 2, 49-52 (1983).
- "Gamma-Ray Imaging with a Rotating Hexagonal Uniformly Redundant Array," Cook, W. R et al., *IEEE Trans. Nuclear Sci.* NS-31, 771-775 (1984).
- "Elemental Composition of Solar Energetic Particles," Cook, W.R. et al., *Ap. J.* 279, 827-838 (1984).
- "Temporal Variations of the Anomalous Oxygen Component," Cummings, A. C. and W. R. Webber, *Proceedings of Solar Wind V Conference, NASA CP 2280*, 435-440 (1983).
- "Short and Long Term Variations of the Anomalous Component," Cummings, A.C. et al., *Proceedings of 18th International Cosmic Ray Conference, Bangalore, India* (1983 in press).
- "Energy Resolution Enhancement of Mercuric Iodide Detectors," Finger, M. et al., *IEEE Transaction on Nuclear Science* NS-31, 348-352 (1984).
- "The Cosmic-Ray Abundances of the Platinum-Lead Elements as Measured on HEAO-3," Fixsen, D.J. et al., *Proceedings of 18th International Cosmic Ray Conference, Bangalore, India* (1983 in press).
- "The Non-Z<sup>2</sup> Response of the Heavy Nuclei Cosmic Ray Detector on HEAO-3," Garrard, T. L. et al., *Proceedings of 18th International Cosmic Ray Conference, Bangalore, India* (1983 in press).
- "Energetic Oxygen and Sulfur Ions in the Jovian Magnetosphere and their Contributions to the Auroral Excitation," Gehrels, N. and E.C. Stone, *Proceedings of 5th Conf. on the Physics of the Jovian and Saturnian Magnetospheres* (1983).
- "Energy Spectra of Ultraheavy Cosmic Rays Results from HEAO-3," Israel, M.H. et al., *Proceedings of 18th International Cosmic Ray Conference, Bangalore, India* (1983 in press).
- "Correlation of Source Abundances of Ultraheavy Cosmic Rays with First Ionization Potential - Results from HEAO-3," Israel, M.H. et al., *Proceedings of 18th International Cosmic Ray Conference, Bangalore, India* (1983 in press).
- "Abundances of 'Secondary' Elements Among the Ultraheavy Cosmic Rays - Results from HEAO-3," Klarmann, J. et al., *Proceedings of 18th International Cosmic Ray Conference, Bangalore, India* (1983 in press).
- "The Relative Abundances of Sn, Te, Xe, Ba, and Ce in the Cosmic Radiation," Krombel, K., *Ph.D. Thesis, CIT* (1983).
- "An Accelerator Test of Semi-Empirical Cross-Sections," Lau, K.H. et al., *Proceedings of 18th International Cosmic Ray Conference, Bangalore, India* (1983 in

press).

- "A Search for  $^2\text{H}$ ,  $^3\text{H}$ , and  $^3\text{He}$  in Large Solar Flares," Mewaldt, R.A. and E.C. Stone, *EOS Tran. AGU Nov.* **64**, 791 (1983).
- "The Elemental and Isotopic Composition of Galactic Cosmic Ray Nuclei," Mewaldt, R. A., *Rev. Geophys. Space Phys.* **21**, 295-305 (1983).
- "Further Isotopic Studies of Heavy Nuclei in the 9/23/78 Solar Flare," Mewaldt, R. A. et al., *Proceedings of 18th International Cosmic Ray Conference, Bangalore, India* **4**, 42-45 (1983).
- "A Search for Deuterium, Tritium and  $^3\text{He}$  in Large Solar Flares," Mewaldt, R.A. and E.C. Stone, *Bull. Am. Phys. Soc.* **28**, 742 (1983).
- "A Search for  $^2\text{H}$ ,  $^3\text{H}$ , and  $^3\text{He}$  in Large Solar Flares," Mewaldt, R. A. and E. C. Stone, *Proceedings of 18th International Cosmic Ray Conference, Bangalore, India* **4**, 52-55 (1983).
- "Deuterium,  $^3\text{He}$ , and Anomalous H and He Nuclei," Mewaldt, R.A. and E.C. Stone, *Proceedings of 18th International Cosmic Ray Conference, Bangalore, India* **2**, 42 (1983).
- "The Isotopic Composition of the Anomalous Low-Energy Cosmic Rays," Mewaldt, R.A. et al., *Ap. J.* (1983 Submitted).
- "A High Resolution Study of the Isotopes of Solar Flare Nuclei," Mewaldt, R.A. et al., *Ap. J.* (1984 in press).
- "The Non-Z<sup>2</sup> Response of the Heavy Nuclei Cosmic Ray Detector on HEAO-3," Newport, B.J. et al., *Bull. Am. Phys. Soc.* **28**, 755 (1983).
- "The Time History of 2.22 MeV Line Emission in Solar Flares," Prince, T.A. et al., *Proceedings of 18th International Cosmic Ray Conference, 4*, 79-82 (1983).
- "The Energetic Particle and Photon Component of Solar Flares," Prince, T.A., *Bull. Am. Phys. Soc.* **29**, 71 (1983).
- "Calibration of An Aerogel Counter of Index 1.1 at the Bevalac," Rasmussen, I. L. et al., *Proceedings of 18th International Cosmic Ray Conference, Bangalore, India* **8**, 77-80 (1983).
- "Calibration of a Stack of NaI Scintillators at the Berkeley Bevalac," Schindler, S. M. et al., *Proceedings of 18th International Cosmic Ray Conference, Bangalore, India* **8**, 73-76 (1983).
- "The Voyager Mission: Encounters with Saturn," Stone, E.C., *J. Geophys. Res.* **88**, 8369 (1983).
- "Cosmic Ray  $^2\text{H}$ ,  $^3\text{H}$ , and Anomalous H and He Nuclei," Stone, E.C. and R.A. Mewaldt, *Bull. Am. Phys. Soc.* **28**, 742 (1983).
- "Cosmic-Ray Abundances of the Even Charge Elements from  $^{50}\text{Sn}$  to  $^{58}\text{Ce}$  Measured on HEAO-3," Stone, E.C. et al., *Proceedings of 18th International Cosmic Ray Conference, Bangalore, India* (1983 in press).
- "Voyager Measurements of the Energy Spectrum, Charge Composition, and Long Term Temporal Variations of the Anomalous Components in 1977-1982," Webber, W. R. and A. C. Cummings, *Proceedings of Solar Wind V Conference, NASA CP 2280*, 427-434 (1983).
- "Studies of Low Energy Cosmic Rays - The Anomalous Component," Webber, W.R. et al., *Proceedings of 18th International Cosmic Ray Conference, Bangalore, India* (1983 in press).